Connections between Density Waves in Fluidized Beds and Compressible Flows

Jayati Johri and Benjamin J. Glasser
Dept. of Chemical and Biochemical Engineering, Rutgers University, Piscataway, NJ 08854

Under certain simplifying assumptions, model equations of motion and continuity for the particles in a fluidized bed can be related to those of a compressible fluid acted on by a density dependent force. A linear stability analysis shows that the base state of the compressible flow equations can lose stability in the form of plane density waves. The plane waves emerge through a Hopf bifurcation and propagate through the bed as traveling waves. Through a bifurcation analysis coupled with parameter continuation, the solution structure of the fully-developed plane waves was computed. As the amplitudes of the plane waves increase, they lose stability in the lateral direction. A comparison of these results with previous work on gas-fluidized beds shows that salient features of the instability of a gas-fluidized bed are captured by the basic physics of compressible flows.

Introduction

In some gas-fluidized beds it is possible to expand the bed homogeneously or uniformly for some flow rate interval beyond that corresponding to minimum fluidization (Geldart, 1986; Tsinontides and Jackson, 1993). However, from the earliest applications of gas-fluidized beds, it was recognized that the uniformly fluidized bed was only one possible flow regime. In most gas-fluidized beds, voidage waves were observed to form and move through the bed. For low flow rates of gas, the voidage waves take on the form of single bubbles of gas that pass upwards through the bed. The bubbles of gas are easily observed as they have dimensions that are many orders of magnitude larger than the particles. As discussed by Daw et al. (1995), the length scales of the bulk or macroscopic motion are typically three orders of magnitude larger than the length scales of individual particle or microscopic motion. In narrow beds, the voids span the width of the column and alternating bands of high and low particle concentration are observed (slugs). At high gas flow rates, bubbles constantly coalesce and break up which leads to complex bubble dynamics. At even higher flow rates, voids of elongated shapes, as well as clusters of particles, move about violently in the bed (Kunii and Levenspiel, 1991; Fan and Zhu, 1998; Jackson, 2000).

The occurrence of voidage or density waves such as bubbles, slugs, and clusters in fluidized beds is an intriguing phenomenon which is still not completely understood (Geldart, 1986; Homsy, 1998; Jackson, 2000). Fluidized-bed reactors are widely used in industry and the occurrence of such waves can have a significant effect on the economics, safety, and environmental impact of a reactor (Kunii and Levenspiel, 1991). In general, some voidage structures only occur for sufficiently large beds so this can lead to difficulties with the scale-up of such beds. The variety of possible flow regimes in fluidized beds can lead to further difficulties with scale-up because the gas and solids mixing rates and gas bypassing, as well as other pertinent quantities, all vary as the flow regime changes.

Continuum mechanics arguments have been used to develop equations of motion to describe the flow of fluid and particles in fluidized beds (see, for example, Anderson and Jackson, 1967, 1968; Garg and Pritchett, 1975; Batchelor, 1988; Jackson, 1997, 2000). Anderson and Jackson (1968) used a linear stability analysis to show that the uniform state (or a uniformly fluidized bed) can become unstable and small disturbances can grow into voidage (or density) waves. More recently, Koch and Sangani (1999) used a kinetic theory approach to predict the particle pressure in concentrated suspensions and then performed a linear stability analysis about the uniformly fluidized state to determine the stability limits.

Since a linear stability analysis can only capture phenomena at small wave amplitudes close to the uniform state, the question of whether or not disturbances in an unstable bed will actually grow into bubble-like solutions has been investigated by taking nonlinear terms into account (Needham and Merkin, 1983, 1986; Liu, 1983; Ding and Gidaspow, 1990;

Correspondence concerning this article should be addressed to B. J. Glasser.

Anderson et al., 1995). Through consideration of the nonlinear terms in the equations of motion, Needham and Merkin (1983) established the existence of a quasi-steady periodic state at flow rates for which the bed is unstable. Needham and Merkin (1986) examined the temporal stability of these quasi-steady periodic state solutions and showed that they were only stable under a limited range of conditions. The recognized importance of the nonlinear terms has also led to the use of a bifurcation approach (using nonlinear dynamics) to investigate the waveforms in fluidized beds (see Childress and Spiegel, 1975; Göz, 1992, 1995; Glasser et al., 1996, 1998). Göz (1992) applied such an approach to examine the instability of fluidized beds and showed how the various parameters affect the evolution of traveling waves from the uniformly fluidized state.

A number of people have pursued the description of bubbles as shocks in one-dimension (Wallis, 1969; Fanucci et al., 1979; Verloop and Heertjes, 1970; Pigford and Baron, 1965; Bouillard and Gidaspow, 1991; Harrison and Crighton, 1994). Wallis (1969) showed that shock waves are formed when the velocity of disturbances exceeds the dynamic wave velocity. Fanucci et al. (1979) analyzed the equations of motion using the method of characteristics and showed that a shock discontinuity arose. They speculated that the shock fronts physically manifest themselves as bubbles. Bouillard and Gidaspow (1991) derived a criterion for bubbling using shock theory, and showed that the interval of stability in uniformly fluidized beds may be influenced by the relative contributions of the interphase drag and solid phase compressibility.

Batchelor and Nitsche (1991) discussed that a dispersion of small particles in a fluid with nonuniform concentration can behave dynamically like a continuum with nonuniform density in certain circumstances. By examining the instability of stratified fluid, they were able to gain insight into the instability of a fluidized bed. It was shown that in sufficiently large systems, there is a global instability which is present no matter how small the variation of density in the undisturbed state. Batchelor (1991) postulated various stages during the process of bubble formation. The first stage is the primary instability of the uniform state which leads to plane waves. A secondary instability follows, which leads to lateral concentration variations. Finally, particles are expelled from the buoyant compact region of smaller concentration which leads to the development of a bubble (see Batchelor and Nitsche, 1994).

As discussed by Jackson (1997), the momentum balances for the gas and particles in fluidized beds lead to a set of equations which must be closed; a common way to close these equations is to adopt constitutive relations. Constitutive relations that are adopted for the drag force lead to a nonlinear coupling of the motion of the gas and solids. This coupling makes it difficult to decipher the role of the gas or solids in the development, growth, and propagation of voidage waves. In addition, a large number of terms appear in the equations of motion and closures, leading to a rather complex model describing the flow. In a review of the models that have been used to study fluidized beds, Jackson (1994) concluded, "...I reemphasize that, for practical purposes, the goal is a set of equations which is good enough to describe the behavior of a range of situations of interest, to acceptable engineering accuracy. Perhaps then our objective should be to seek how much can be left out, while still meeting this criterion, rather than attempting to include every conceivable term." Meeting this goal requires a rigorous understanding, both qualitative and quantitative, of the role played by the various terms that are commonly incorporated into continuum models. By considering simplified equations of motion that we are able to uncouple, to some extent, the flow of the gas and particles. In particular, we can show that much of the physics of the bed may be understood by examining the solids equations with the gas providing a density dependent force (which prevents the solids from settling under gravity).

In this work, we show that a fluid of variable density acted upon by a density dependent force exhibits the same primary and secondary instability as is seen in a gas-fluidized bed. We will first show that under certain simplifying assumptions the solution of the equations of motion and continuity for the gas and particles in a fluidized bed can be related to the solution of equations for a fluid with variable density. While we believe the instability of a compressible fluid with a density dependent force is an interesting problem in itself, our main motivation for such an analysis is to gain insight into density waves in fluidized beds.

A wave hierarchy approach was used by Needham and Merkin (1984a) to study the solution of a generalized set of equations of motion which arise in a variety of physical situations such as roll waves in inclined channels (Needham and Merkin, 1984b), as well as traffic flows. They showed that the linearized steady-state condition is the same as that predicted by Whitham (1974) and set forth the conditions in which the uniform state develops supercritical, subcritical, and degenerate bifurcations. While the reference to fluidized beds, as well as compressible flows, is implicit in their work, we have examined the connections between the equations of motion used to study fluidized beds, the 1-D equations studied by Needham and Merkin (1984a), and those arising in compressible flows.

We present our findings of a linear stability analysis of the uniform state (of the compressible flow equations), and we find that the uniform state can lose stability in the form of plane waves. The waves emerge through a Hopf bifurcation of the base state which occurs at a Mach number of one. We then go on to examine the system using a bifurcation analysis of the traveling wave solutions in order to examine the form and solution structure of the waves. The waves are sinusoidal in shape at low amplitudes, but become increasingly asymmetrical as their amplitude increases. A stability analysis shows that these waves lose stability in the lateral direction much like the waves in a stratified fluid of variable density. Finally, we compare these results with previous work on gas-fluidized beds to discuss the effects of using the single-phase approach to modeling these systems.

Model Equations

Modeling the flow of gas and particles in a fluidized bed as the flow of a fluid of variable density acted upon by a density-dependent force may seem like a gross simplification of the system. However, as was discussed in the introduction, a suspension of small particles with nonuniform concentration can sometimes behave like a continuum with nonuniform density. Moreover, it is of interest to compare the results obtained from the simplified model and the two-phase model.

Volume-averaged equations of continuity and motion for the gas and particle phases of a gas-particle suspension can be written as (Anderson and Jackson, 1967)

$$\frac{\partial \phi}{\partial t} + \nabla\cdot(\phi \boldsymbol{u}_s) = 0 \tag{1}$$

$$\frac{\partial (1-\phi)}{\partial t} + \nabla\cdot\left[(1-\phi)\boldsymbol{u}_g\right] = 0 \tag{2}$$

$$\rho_s \phi\left[\frac{\partial \boldsymbol{u}_s}{\partial t} + \boldsymbol{u}_s\cdot\nabla\boldsymbol{u}_s\right] = -\nabla\cdot\boldsymbol{\sigma}_s - \phi\nabla\cdot\boldsymbol{\sigma}_g + k\tilde{\boldsymbol{f}} + \phi\rho_s\boldsymbol{g} \tag{3}$$

$$\rho_g(1-\phi)\left[\frac{\partial \boldsymbol{u}_g}{\partial t} + \boldsymbol{u}_g\cdot\nabla\boldsymbol{u}_g\right] = -(1-\phi)\nabla\cdot\boldsymbol{\sigma}_g - k\tilde{\boldsymbol{f}} + (1-\phi)\rho_g\boldsymbol{g} \tag{4}$$

where it has been assumed that the gas is incompressible and the gas-particle suspension is isothermal. ϕ is the local average volume fraction of solids, $\boldsymbol{u}_g$ and $\boldsymbol{u}_s$ are the local average gas and solids velocities, respectively, $\boldsymbol{\sigma}_g$ and $\boldsymbol{\sigma}_s$ are the gas and solid phase stress tensors, k is the number of particles per unit volume, $\tilde{\boldsymbol{f}}$ is the average force exerted on a particle by the gas due to the relative motion between the phases, and $\boldsymbol{g}$ is the gravity force vector.

In order to the close the equations of motion we adopt closures motivated by Anderson and Jackson (1968). Since we are considering gas-fluidized beds, we will ignore virtual mass effects and model the interaction force $\tilde{\boldsymbol{f}}$ as interphase drag. The interphase drag force can be written as (Richardson and Zaki, 1954)

$$k\tilde{\boldsymbol{f}} = (1-\phi)\beta(\boldsymbol{u}_g - \boldsymbol{u}_s) \tag{5}$$

where β is a function of the solids fraction and the Reynolds number, $R_t = 2av_t\rho_g/\mu_g$; v_t is the terminal velocity of fall of a particle of radius a. A form analogous to that of a Newtonian fluid will be assumed for the gas-phase stress tensor (Anderson and Jackson, 1968)

$$\boldsymbol{\sigma}_g = P_g\boldsymbol{I} - \mu_g\left[\nabla\boldsymbol{u}_g + \nabla(\boldsymbol{u}_g)^T - \frac{2}{3}(\nabla\cdot\boldsymbol{u}_g)\boldsymbol{I}\right]$$

where P_g and μ_g are the gas-phase pressure and viscosity, respectively.

Continuum mechanics arguments (Anderson and Jackson, 1968) or the kinetic theory of dense gases (see, for example, Ding and Gidaspow, 1990; Dasgupta et al., 1994; Hrenya and Sinclair, 1997) provide a constitutive relation for $\boldsymbol{\sigma}_s$, in terms of the rate of deformation of the particle phase

$$\boldsymbol{\sigma}_s = P_s\boldsymbol{I} - \mu_s\left[\nabla\boldsymbol{u}_s + \nabla(\boldsymbol{u}_s)^T - \frac{2}{3}(\nabla\cdot\boldsymbol{u}_s)\boldsymbol{I}\right]$$

where P_s is the isotropic component of the stress (that is, the particle pressure) and μ_s is the effective viscosity of the particle phase. In this case, the stress $\boldsymbol{\sigma}_s$ represents the resistance to deformation of the particle assembly arising from particle-particle interactions. A kinetic theory closure would require an additional field equation for the pseudo-thermal energy since P_s and μ_s would be functions of the mean particle fluctuation velocity (granular temperature) in addition to the solids fraction. However, since our goal is to simplify the model, we will not consider a kinetic theory closure, but rather consider the simplest possible closures for P_s and μ_s (capable of capturing the instability of a fluidized bed). This is equivalent to assuming that the particle fluctuation velocity or granular temperature is a constant throughout the bed. It is clear that in general this will not be the case; but it has already been shown for the two-phase equations that a model with a viscosity and pressure that are independent of temperature is capable of capturing the instability of a fluidized bed (Anderson and Jackson, 1968). Thus, we have used this two-phase model as a starting point for our analysis. In any event, the exact forms for P_s and μ_s are not needed at this stage of our analysis, so the particle pressure will be taken to be a monotonically increasing function of the solids fraction

$$P_s = \overline{P}_s\gamma_1(\phi); \qquad \frac{d\gamma_1}{d\phi} > 0; \tag{6}$$

and the viscosity of the particle phase will be taken to be a constant or increasing function of the solids fraction

$$\mu_s = \overline{\mu}_s\gamma_2(\phi); \qquad \frac{d\gamma_2}{d\phi} \geq 0. \tag{7}$$

$\overline{P}_s$ and $\overline{\mu}_s$ are dimensional prefactors for the particle pressure and viscosity, respectively. Depending on the chosen functional forms for P_s and μ_s, they can either represent the particle pressure and viscosity at some reference state, or have values of unity with units of pressure and viscosity, respectively. With suitable functional forms for P_s and μ_s, the equations of motion and continuity are closed and solutions can be found. This formulation also assumes that the solids stress can be decoupled from that of the fluid stress. This assumption has been made by a large number of researchers examining fluidized beds (see, for example, Göz, 1995 and references therein) and its validity has been discussed by Jackson (1997). In general this assumption is not good for a very dilute gas-particle flow, and, thus, it may not be a good approximation for the gas-rich region in the center of a bubble.

The density and viscosity of a gas are both small near ambient conditions, so the equations of motion (3 and 4) can be further simplified. This can be done by neglecting terms of the order of the gas-phase density relative to those of the order of the solid-phase density, and similarly neglecting terms of the order of the gas-phase viscosity relative to those of the order of the solid-phase viscosity. In general, the density of the gas-particle suspension will be given by $\rho = \rho_s\phi + \rho_g(1-\phi)$ which can be approximated as $\rho = \rho_s\phi$ for $\rho_g \ll \rho_s$. With the above simplifications, Eqs. 3, 4, and 5 can be combined to obtain (Jackson, 1994)

$$\nabla P_g + \beta(\boldsymbol{u}_g - \boldsymbol{u}_s) = 0 \tag{8}$$

$$\rho_s\phi\left[\frac{\partial \boldsymbol{u}_s}{\partial t} + \boldsymbol{u}_s\cdot\nabla\boldsymbol{u}_s\right] = \beta\left[\boldsymbol{u}_g - \boldsymbol{u}_s\right] - \nabla\cdot\boldsymbol{\sigma}_s + \rho_s\phi\boldsymbol{g} \tag{9}$$

where the first equation describes the percolation of the gas through the particles. The second equation represents the

equation of motion of the particle assembly, and it looks like the equation of motion of a fluid of variable density $\rho = \rho_s \phi$ with effective viscosity μ_s and effective pressure $P_s + P_g$. However, as discussed by Jackson (1994), P_s is determined constitutively, while P_g is determined dynamically so the two equations of continuity are still needed and the solution of Eqs. 8 and 9 is not completely analogous to that of a variable density fluid.

While there is a large body of work investigating instabilities in the above model, it is difficult to decipher the role of the gas or solids in the development, growth and propagation of the voidage waves. Moreover, we are at the point where such equations are routinely used to describe fluidized beds. In many instances, there is a recognized lack of quantitative agreement between such models and experiments, and it is not always clear which terms or closures should be modified in order to obtain quantitative agreement. A simplified model that captures the physics of the system allows us to isolate the key terms and determine how they affect bed behavior.

In order to simplify the equations we will first focus on the base state. An equilibrium solution to the above closed set of equations of motion (Eqs. 8 and 9) and the equations of continuity (Eqs. 1 and 2) is a uniform fluidized bed with

$$\phi = \phi_o; \qquad \boldsymbol{u}_g - \boldsymbol{u}_s = \boldsymbol{j}u_o; \qquad \nabla P_g = \rho_s \phi \boldsymbol{g}; \qquad \beta u_o - \phi_o \rho_s g = 0 \quad (10)$$

where ϕ_o and u_o are constants and $\boldsymbol{j}$ is the unit vector in the x-direction pointing vertically upwards. From the solution above, it can be seen that, for a uniformly fluidized bed, the relative velocity between the gas and solids (or slip velocity) $\boldsymbol{u_g} - \boldsymbol{u}_s$ is a constant equal to $\boldsymbol{j}u_o$. The value of u_o can be calculated from the steady-state condition. If we assume that the slip velocity in the interphase drag term can be replaced by a constant (equal to $\boldsymbol{j}u_o$), even for nonuniformly fluidized beds, then the equations above can be further simplified. The assumption of constant slip velocity has been made in bubble columns (see Sokolichin and Eigenberger, 1999), however, at this point, we will hold off on further discussion of the physical basis for this assumption, and go on to evaluate its ramifications. The equations of continuity and motion for the solids (1 and 3) can then be written as

$$\frac{\partial \phi}{\partial t} + \nabla \cdot (\phi \boldsymbol{u_s}) = 0 \quad (11)$$

$$\rho_s \phi \left[\frac{\partial \boldsymbol{u}_s}{\partial t} + \boldsymbol{u}_s \cdot \nabla \boldsymbol{u}_s \right] = \boldsymbol{F} - \nabla \cdot \boldsymbol{\sigma}_s + \rho_s \phi \boldsymbol{g} \quad (12)$$

where $\boldsymbol{F} = \boldsymbol{j}\beta \boldsymbol{u}_o$, and the solution of the equations of continuity and motion for the solids becomes decoupled from that of the gas. The gas motion becomes trivially linked to the motion of the solids and the local solids fraction through the equation of continuity of the gas. If we assume μ_s to be a constant (although this restriction can easily be relaxed), then Eqs. 11 and 12 are the equations of continuity and motion of a Newtonian fluid with variable density $\rho = \rho_s \phi$ and viscosity μ_s. They can therefore be rewritten as

$$\frac{\partial \rho}{\partial t} + \nabla \cdot (\rho \boldsymbol{v}) = 0 \quad (13)$$

$$\rho \left[\frac{\partial \boldsymbol{v}}{\partial t} + \boldsymbol{v} \cdot \nabla \boldsymbol{v} \right] = \boldsymbol{F} - \nabla \cdot \boldsymbol{\sigma} + \rho \boldsymbol{g} \quad (14)$$

where $\boldsymbol{v} = \boldsymbol{u}_s$, $\mu = \mu_s$, $\boldsymbol{\sigma} = \boldsymbol{\sigma}_s$, and $P = P_s$. These are the equations of motion of a Newtonian, compressible fluid where, in addition to the inertial, viscous, pressure, and gravitational forces, we have an additional density dependent force $\boldsymbol{F}$. In order to avoid confusion we will distinguish between this fluid of variable density and the gas (which is of course also a fluid). Thus, when we use the term "fluid", we are making a reference to the above-mentioned fluid of variable density (whose motion can be related to the motion of the solids in a fluidized bed).

We will initially examine the development of density waves in only the vertical (or x) direction in which case the equations simplify to

$$\frac{\partial \rho}{\partial t} + \frac{\partial (\rho v)}{\partial x} = 0 \quad (15)$$

$$\rho \left[\frac{\partial v}{\partial t} + v \frac{\partial v}{\partial x} \right] = -\frac{\partial P}{\partial x} + F + \mu \left(\frac{4}{3} \right) \frac{\partial^2 v}{\partial x^2} - \rho g \quad (16)$$

where we define $v = v_x = \boldsymbol{j} \cdot \boldsymbol{v} = u_{x,s}$ as the x-component of the velocity vector and $F = F_x = \boldsymbol{j} \cdot \boldsymbol{F} = \beta u_o$ as the x-component of the density dependent force (where the x-subscripts have been omitted for convenience). At this stage, we will hold off on nondimensionalizing these equations until the next section when scalings relevant to this system can be defined. As discussed, we have not implemented a kinetic theory closure for the solid-phase stress. This is equivalent to assuming that the particle fluctuation velocity or granular temperature is a constant throughout the bed. Thus, the physical scenario being described is analogous to an ideal, isothermal gas, but instead of molecules, the system consists of particles. As would be expected for an ideal, isothermal gas, the pressure P can be expressed as a function of density. The pressure increases with ρ for reasons similar to those in an ideal gas; as the particles (or molecules) get closer together, the isotropic resistance to further compression also increases. Note that the equations considered here can be extended such that they resemble those describing nonisothermal gases by using the kinetic theory of granular materials (which involves a pseudo-thermal energy balance and a closure for the particle pressure and viscosity in terms of the granular temperature).

Similarly, F is only a function of density. As we will discuss later, this force will balance gravity thus allowing for a uniform state (which corresponds to a uniformly fluidized bed). The density dependent force F is assumed to be an increasing function of density since β, the drag coefficient, increases with volume fraction of solids (and, therefore, with density).

These equations represent the starting point for our investigation. The model equations were solved assuming periodic boundary conditions as a first step to understanding the development of density waves in the model system. Jackson (2000) has discussed possible boundary conditions for fluidized beds and further work is needed in order to investigate the effect of boundary conditions on the voidage waves. The stability analysis described in this work is a general examination of the instabilities in a compressible fluid acted

upon by a density dependent force and does not necessarily have to be connected to a fluidized bed. However, we have chosen parameter values which correspond to gas-fluidized beds and some of the closures we have adopted for F and P correspond to suitable closures for gas-fluidized beds.

We first considered the simplest possible (nontrivial) closures for F and P—linearly varying functions of ρ. F is represented by

$$F = A\rho + B \tag{17}$$

where the constants A and B were chosen in accordance with the condition $F_o = \rho_o g$, which holds at the uniform steady state (as explained later in this section). P is represented by

$$P = E\rho \tag{18}$$

where E is a constant. Next, the effect of making the closures nonlinear was examined by using relations for the density dependent force and particle pressure that are based on work in fluidized beds. A suitable form for the density dependent force can be obtained from the Richardson-Zaki (1954) correlation for β

$$\beta = \frac{\phi(\rho_s - \rho_g)g}{v_t(1-\phi)^{n-1}} \tag{19}$$

Since $F = \beta u_o$, we can rewrite this as

$$F = \frac{\rho g u_o}{v_t\left[1-(\rho/\rho_s)\right]^{n-1}} \tag{20}$$

where $u_o = v_t[1-\rho_o/\rho_s]^{n-1}$ and n is the Richardson-Zaki exponent. The value of n may be determined from the relations specified by Richardson and Zaki (1954). The value of the terminal velocity of a single particle v_t was calculated from empirical correlations (Kunii and Levenspiel, 1991).

A nonlinear form of P_s has been considered in this work in addition to the linear closure given in Eq. 18. The nonlinear form for P_s is adopted based on work by Johnson and Jackson (1987) for particulate systems

$$P = P_s = K\frac{\phi^{m_1}}{(\phi_{cp}-\phi)^{m_2}} \tag{21}$$

and we chose $m_1 = 1$ and $m_2 = 2$ such that the value of the volume fraction ϕ is restricted to some maximum value ϕ_{cp} at close packing. The closure represents a particle pressure that is proportional to the density for small values of ϕ. The value of the volume fraction corresponding to close packing is taken to be 0.65 (Berryman, 1982). This form of the solids pressure in terms of the density of the bed $\rho = \rho_s\phi$ is

$$P = \frac{K\rho_s\rho}{(\rho_{cp}-\rho)^2} \tag{22}$$

where $\rho_{cp} = \rho_s\phi_{cp}$.

A spatially uniform steady state exists for Eqs. 15 and 16 and is given by $v = 0$; $\rho = \rho_o$; $F_o = \rho_o g$. This represents a state where the "fluid" (whose motion can be related to the solids) is at rest and the density dependent force balances the gravitational force on the "fluid". The equations of continuity and motion are Galilean invariant so any arbitrary (constant) velocity can be added to the equations without affecting the overall solutions. By stating that the fluid is at rest (for the base state), we have implicitly defined a frame of reference of an observer. This frame of reference corresponds to the laboratory frame of reference where the flux of fluid is zero. In this work we have examined density wave solutions of these equations, taking into account nonlinear effects. By making use of a bifurcation analysis, we have followed the solution structure of these waves.

Linear Stability Analysis

Equations 15 and 16 represent two coupled nonlinear partial differential equations in v and ρ. The fate of small perturbations can be evaluated by carrying out a linear stability analysis of the uniform state, and it can be shown that the growth rate is given by the roots of a quadratic (R. Jackson, 1996, personal communication). The expression is readily obtained by linearizing Eqs. 15 and 16 about the steady state and computing the growth rate of disturbances. This was accomplished by first adding small perturbations, ρ_p and v_p to the steady-state solution such that $\rho = \rho_o + \rho_p$ and $v = v_p$. These perturbed forms of the density and velocity were introduced into Eqs. 15 and 16 and only linear terms were retained. Solutions of the form $\rho_p = \rho_1 e^{st}e^{i\kappa x}$ and $v_p = v_1 e^{st}e^{i\kappa x}$ (where ρ_1 and v_1 are the amplitude of the perturbations) were then introduced into the linear equations. The resulting equations can then be rewritten in the form of a quadratic in the growth rate s. The roots of the quadratic are given by

$$s = \frac{2\mu\kappa^2}{3\rho_o}\left[-1 \pm \sqrt{1 - \frac{9\rho_o^2 P_o'}{4\mu^2\kappa^2} + \frac{9\rho_o^2(F_o'-g)}{4\mu^2\kappa^3}\,i}\right] \tag{23}$$

where $F_o' = \left[\frac{dF}{d\rho}\right]_{\rho_o}$ and $P_o' = \left[\frac{dP}{d\rho}\right]_{\rho_o}$.

Although Needham and Merkin (1984a) derive an equivalent expression for the eigenvalues of the one-dimensional (1-D) equations in terms of the higher and lower order wave speeds, we have carried out a somewhat different (and, to our taste, simpler) derivation which highlights the role of the physical parameters of the system. The resulting growth rate is a function of the parameters ρ_o, μ, F_o', and P_o' and the wave number of the disturbance κ. The growth rate $s = \sigma - i\omega$ is complex indicating that disturbances move through the bed as traveling waves. We are interested in distinguishing between waves that get amplified as they propagate from those that do not, so the real part of the growth rate is plotted as a function of the wave number in Figure 1. Here, the linear closures for F and P (given in Eqs. 17 and 18) have been used with the parameters given in Table 1. Note that for the linear closures, $F_o' = A$ and $P_o' = E$. The parameter values for F can be obtained from empirical correlations for the drag coefficient (Richardson and Zaki, 1954), while those for P can be obtained from measurements of the particle pressure (Jackson, 2000). The parameter values are chosen to be in the right range (as suggested by experiments) for glass

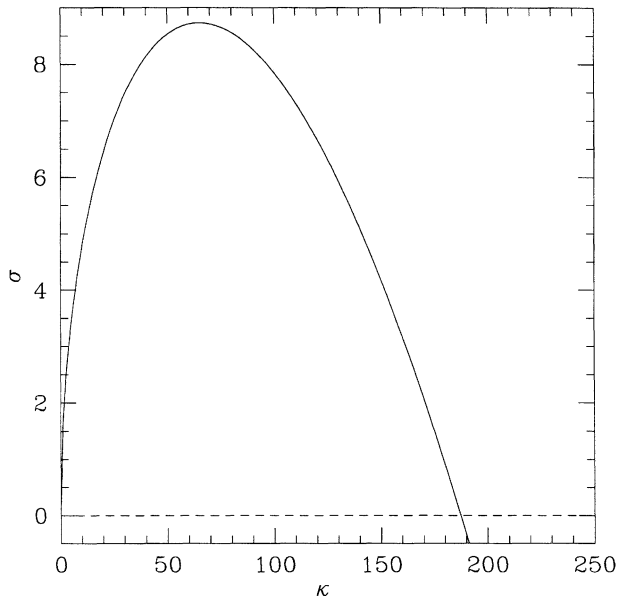

Figure 1. Real part of growth rate (with units of 1/s) vs. vertical wave number (with units of 1/m).

Computed by a linear stability analysis about the uniform state.

beads of a few hundred microns in diameter fluidized by air (Glasser et al., 1996; Jackson, 2000).

As shown in Figure 1, the real part of the growth rate is positive for a range of wave numbers starting from zero, and becomes negative for large values of the wave number. The instability of the uniform state is, thus, a long wave instability. The growth rate curve is characterized by the real part of the growth rate σ starting from zero at a wave number of zero, going through a maximum σ_m and then decreasing to zero again at a critical wave number κ_c. At the critical wave number, a Hopf bifurcation occurs and a pair of complex conjugate eigenvalues cross the imaginary axis. Physically, κ_c represents the boundary between disturbances that will and will not be amplified as they propagate through the bed. The new branch of solutions that is born at this Hopf bifurcation will be discussed in the next section.

The equations are made dimensionless using the velocity of the wave at the Hopf bifurcation point c_b as the reference velocity and the quantity c_b^2/g as the reference length. It is convenient to define a base case for the reference velocity in order to compare systems with different parameter values. To this end, we will take the base case for the reference velocity as the c_b value corresponding to the parameters in Table 1. This value (which is given in Table 1) will be used as a representative velocity to scale the results. The relevant quantities in the equations of motion may be nondimensionalized as follows: $x = (c_b^2/g)x^*$, $\rho = \rho_o \rho^*$, $t = (|c_b|/g)t^*$, $v = |c_b|v^*$, $P = \rho_o c_b^2 P^*$ and $F = \rho_o g F^*$ (where the starred quantities are dimensionless).

Table 1. Parameter Values for the Linear Closures

ρ_o	1,100 kg/m^3
μ	0.665 kg/(m·s)
A	14.7 m/s^2
E	0.03 J/kg
c_b	−0.173 m/s

Equations 15 and 16 can be rewritten in dimensionless form as

$$\frac{\partial \rho^*}{\partial t^*} + \frac{\partial [\, \rho^* v^*]}{\partial x^*} = 0 \tag{24}$$

$$\rho^* \left[\frac{\partial v^*}{\partial t^*} + v^* \frac{\partial v^*}{\partial x^*} \right] = F^* - \frac{\partial P^*}{\partial x^*} + \frac{4}{3} \frac{1}{\Omega} \frac{\partial^2 v^*}{\partial x^{*2}} - \rho^* \tag{25}$$

where $\Omega = (\rho_o c_b^3)/(g\mu)$. Note that choosing a length scale of c_b^2/g implies that the Froude number is always equal to one. While this may seem restrictive at first glance, we believe this is a good approximation of the regime we are interested in, since this length scale leads to the scaling of F by $\rho_o g$ which is in line with our uniform steady-state solution. While there are other ways to scale the equations, we have used the quantities given above as they are representative of the flow at the base state.

It is of interest to examine the effect of varying the parameters on the stability of the bed. The predictions of the model can then be compared with physical observations, as well as the predictions of the linear stability analysis carried out using the two-phase model (Anderson and Jackson, 1968; Hernandez and Jimenez, 1991; Anderson et al., 1995). In Figure 2a the real part of the dimensionless growth rate σ^* is plotted vs. the dimensionless wave number κ^*. The growth rate and wave number have been made dimensionless using the following scalings: $\sigma^* = \sigma|c_b|/g$ and $\kappa^* = \kappa c_b^2/g$ where c_b is chosen to be the value of the velocity at the bifurcation point (see Table 1).

Figure 2a shows the effect of varying the gradient in the density dependent force F_o'. As curve I shows, when the value of F_o' is equal to g, the bed is always stable. For any value of F_o' not equal to the gravitational acceleration, the bed is unstable. It should be noted that the gradient in the density dependent force does not appear by itself in the growth rate equation (see Eq. 23), but it is rather combined with gravity in the form of $(F_o' - g)$. The expression $(F_o' - g)$ in turn appears under the square root and this leads to the situation where the real component of the growth rate σ^* is a function of the quantity $|F_o' - g|$. Hence, σ^* vs. κ^* curves corresponding to F_o' values of 0.5 g and 1.5 g, for example, are identical.

Figure 2b illustrates the direction of propagation of the instabilities, where $c^* = c/c_b = \omega/(c_b\kappa)$. Curves I through IV in Figure 2b (which correspond to F_o' values greater than g) involve only negative values of c which represent a downward direction of propagation. (Figure 2b involves positive values of c^* because c has been nondimensionalized through division by c_b which is also negative in this case.) In general, when $F_o' > g$, values of ω are negative such that the unstable root has a positive imaginary part, that is, $s = \sigma + i|\omega|$ and the perturbation can be represented as a wave which grows in amplitude and propagates downward. When $F_o' < g$, values of ω are positive such that the unstable root has a negative imaginary part $s = \sigma - i|\omega|$ and the perturbation can be represented as a wave which grows in amplitude and propagates upward.

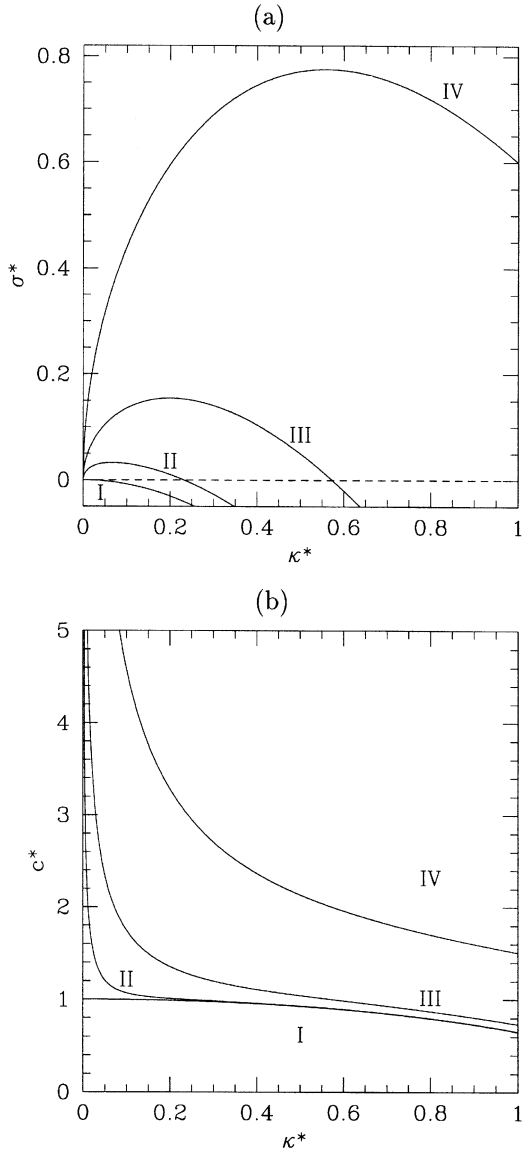

Figure 2. Effect of varying parameter F_o' on stability of the uniform steady state.

(a) Real part of growth rate vs. wave number; (b) phase velocity vs. wave number. (I) $F_o' = 9.8$ m/s^2; (II) $F_o' = 10.6$ m/s^2; (III) $F_o' = 14.7$ m/s^2; (IV) $F_o' = 50.0$ m/s^2.

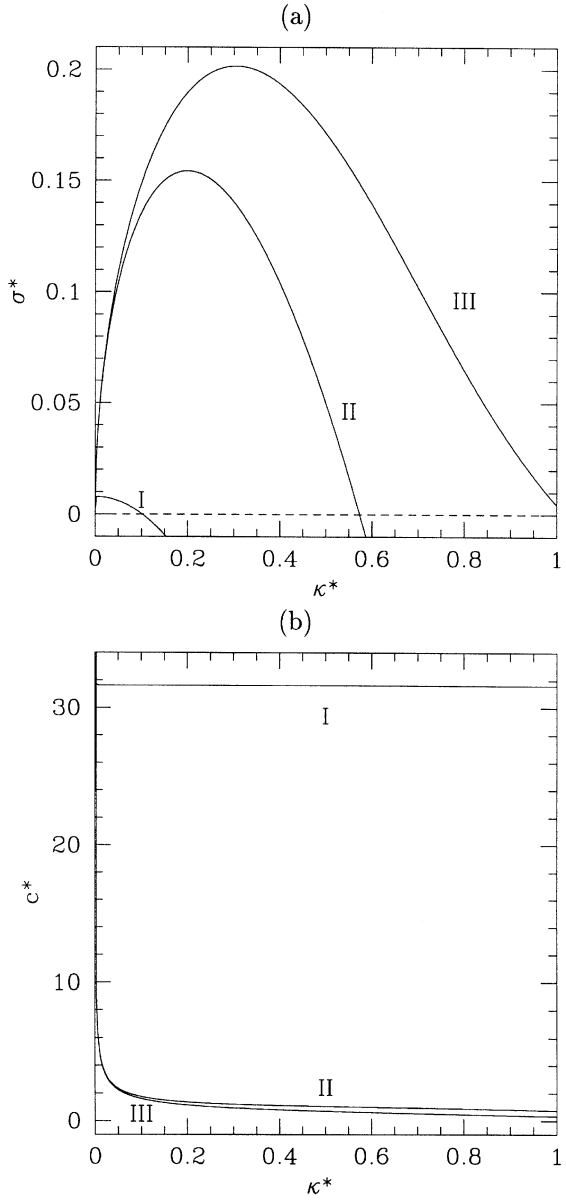

Figure 3. Effect of varying parameter P_o' on stability of the uniform state.

(a) Real part of the growth rate vs. wave number; (b) phase velocity vs. wave number. (I) $P_o' = 30.0$ J/kg; (II) $P_o' = 0.030$ J/kg; (III) $P_o' = 0.003$ J/kg.

Although any value of F_o' not equal to g leads to an unstable bed, the physical meaning of the solution is different depending on whether or not F_o' is less than or greater than g. The magnitude of the phase velocity is the same for a given value of $|F_o' - g|$, that is, only the direction of propagation depends on the actual value of F_o' relative to g. As before, this occurs as the gradient in the density dependent force is combined with gravity in the form of $(F_o' - g)$ in the growth rate equation (see Eq. 23). Since the instability is governed by the sign and magnitude of $(F_o' - g)$, a change in the gravitational acceleration is equivalent to changing F_o'. Thus, the results in Figure 2 can also be interpreted in terms of changing the gravitational acceleration with F_o' held constant. When the nonlinear form of F described in Eq. 20 is used, F_o' itself is a function of the gravitational acceleration; that is, F_o' increases monotonically with g. This leads to progressively less stable beds as the value of g is increased and the bed is unstable for any value of g not equal to zero.

The influence of the parameter P_o', which is related to the compressibility of the "fluid" is shown in Figure 3a. The bed becomes more stable as the gradient in the pressure increases, that is, the critical wave number and the maximum growth rate both decrease as P_o' increases. Figure 3b shows the effect of P_o' on the phase velocity. Note that although the wave speed at the bifurcation varies with P_o', all three curves in Figure 3 have been scaled through division by the value of c_b given in Table 1; the parameters pertaining to this case

correspond to curve II and are given in Table 1. This was done in order to avoid distorting the relative magnitudes of the three curves. On examination of the magnitude of the changes caused by changing the model parameters, it is clear that the parameter P_o' has by far the largest effect on the phase velocities of the waves. Indeed, it can be shown (using the basic principles of fluid mechanics and sound propagation) that the velocity of the wave at the bifurcation (which occurs at the critical wave number κ_c^*) is determined solely by the parameter P_o'. The Mach number for this system is given by $M = c_b/a$ where a is the isothermal speed of sound in the medium. It is known that the velocity of an infinitesimal disturbance in a fluid is also the acoustic velocity in that fluid. In this case, the "fluid" motion can be related to the motion of the solids in a fluidized bed (see the previous section). This velocity can be determined from a simple momentum balance over a control volume which leads to the result $a^2 = dP/d\rho$ where $dP/d\rho$ is related to the bed's resistance to compression (Pai and Luo, 1991). It was seen that the wave speed at κ_c^* is always equal to $\sqrt{P_o'}$. Therefore, the bifurcation occurs at a Mach number of 1 and these solutions are supersonic disturbances that arise from an inertial instability. These results are in accordance with those of Needham and Merkin (1986) who analyzed the two-phase equations using analytic methods. They showed that a Hopf bifurcation occurred at a critical wave speed equal to $\sqrt{P'(\rho_o)}$ and that no bifurcation occurs if this value is set to zero.

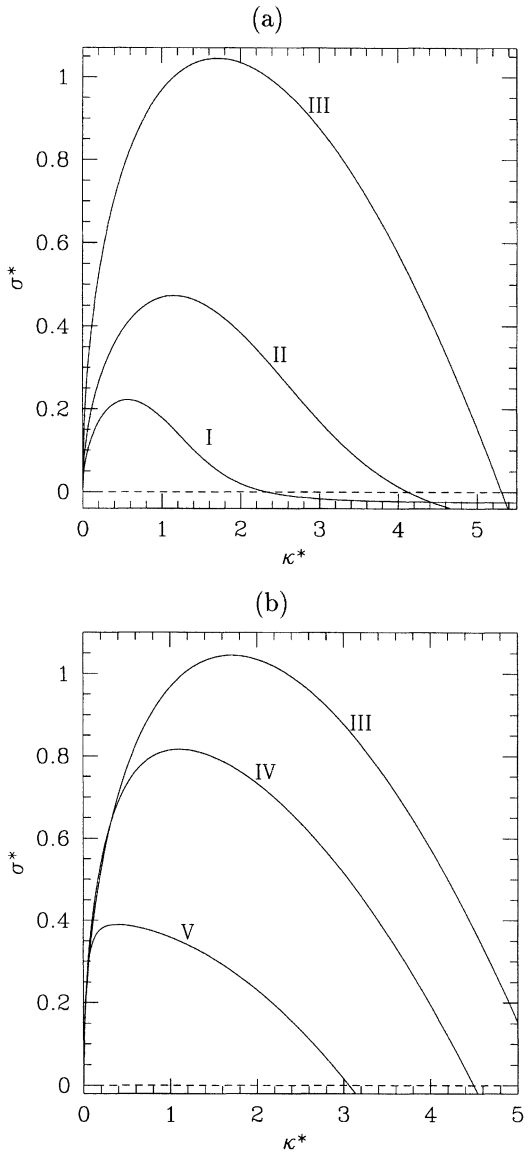

Figure 4. Linear stability analysis using nonlinear closures for *F* and *P*.

The real part of the growth rate vs. wave number for varying values of the density at the uniform state. (a) Dilute beds; (b) dense beds. (I) $\rho_o = 220$ kg/m^3, (II) $\rho_o = 440$ kg/m^3, (III) $\rho_o = 1{,}100$ kg/m^3, (IV) $\rho_o = 1{,}210$ kg/m^3, (V) $\rho_o = 1{,}320$ kg/m^3.

Then, the viscosity was varied over two orders of magnitude. It was observed that the bed becomes more stable as the viscosity of the bed increases. This might be expected since viscous forces resist the motion of a disturbance and damp out disturbances with large wave numbers. It should be noted that a linear stability analysis of the uniformly fluidized bed for the two-phase model has shown that viscous effects introduce a maximum in the plot of the growth rate vs. wave number (Jackson, 1963; Anderson and Jackson, 1968). The linear stability analysis carried out by Anderson and Jackson (1968) on the two-phase model showed that if the viscous term was not included, the growth rate increases without bound for large wave numbers in unstable beds. This is also observed in the current work for a fluid of variable density.

Similarly, the density was varied over several orders of magnitude. It was seen that the bed becomes progressively more unstable as ρ_o is increased. This trend is in contrast to results seen by Anderson and Jackson (1968) where the density was observed to exert a stabilizing influence. It will now be shown that this trend is caused by the linear closure for the pressure, which does not reflect the physics of concentrated suspensions such as fluidized beds.

Figure 4 shows the results for the nonlinear closures for F and P in Eqs. 20 and 22 with the parameters given in the first column of Table 2. The parameters were chosen to represent 100 micron glass beads fluidized in air, because they are in the Geldart A regime and do have a state of homogenous fluidization (Kunii and Levenspiel, 1991). The density (or volume fraction) of the uniform state was varied to include values corresponding to dense and dilute fluidized beds

Table 2. Parameter values*

$2a$	0.0001 m	0.0002 m
ρ_s	2,200 kg/m^3	2,200 kg/m^3
ϕ_p	0.65	0.65
ρ_o	1,100 kg/m^3	1,254 kg/m^3
ρ_g	1.3 kg/m^3	1.3 kg/m^3
μ	0.665 kg/(m·s)	0.665 kg/(m·s)
μ_g	1.81×10^{-5} kg/(m·s)	1.81×10^{-5} kg/(m·s)
n	3.91	4.35
R_t	3.64	20
v_t	0.507 m/s	1.42 m/s
m_1	1	1
m_2	2	2
K	1.08 Pa	1.08 Pa

*Values in column 1 pertain to 100 micron glass beads in air and were used with nonlinear closures. Values in column 2 pertain to 200 micron glass beads in air and were used with the two-phase model.

and those in between. Figure 4a shows the trend in the growth rate obtained with densities (or volume fractions) representing dilute beds. Although the values of P_o' and, therefore, c_b vary with ρ_o, the same value of c_b (the value obtained for $\rho_o = 1{,}100$ kg/m^3) is used to scale the curves in order to avoid distorting the relationship between the curves. At low densities, the bed becomes more unstable with an increase in density, that is, the maximum growth rate σ_m and critical wave number κ_c^* both increase with density. This trend continues until a critical density $\hat{\rho}$ of 946 kg/m^3. (The corresponding critical wave number for the $\rho = \hat{\rho}$ curve will be termed $\hat{\kappa}_c^*$.) At this point, a further increase in density leads to the bed becoming more stable, that is, the maximum growth rate and critical wave number now decrease with density (see Figure 4b). Thus, $\hat{\kappa}_c^*$ represents the maximum wave number for which an instability can be found. For any wave number less than $\hat{\kappa}_c^*$, there will be two possible Hopf bifurcations: one which corresponds to a fluid density below $\hat{\rho}$, a low density instability, and one which corresponds to a density above $\hat{\rho}$, a high density instability. These results are in contrast to the trend obtained using the linear closures where the critical wave number always increased with density.

The existence of a high density and low density instability has been observed for the two phase equations describing fluidized beds (Glasser et al., 1998). The low density instability was associated with the development of cluster-like solutions (localized regions of higher than average density surrounded by regions of low density), while the high density instability was associated with the development of bubble-like solutions (localized regions of lower than average density surrounded by regions of higher density).

We have seen that the existence of an upper and lower instability point is a result of the nonlinear closure for P. Specifically, we find that only the low density instability is captured with the linear closure for P (that is, using Eq. 18) and the nonlinear closure for F (that is, using Eq. 20). However, both the high and low density instabilities are observed with the linear form of F (Eq. 17) and the nonlinear form for P (Eq. 22).

The occurrence of the high and low density instabilities can be understood based on the role that the pressure closure plays in governing the stability of the bed. Consider the effect of increasing the density of the bed at the base state. The inertial terms which drive the instability will increase with an increase in density; thus, the base state will tend towards becoming more unstable with an increase in density. The gradient of pressure with respect to density P' ($= dP/d\rho$) serves as a stabilizing force. (P' represents the isotropic resistance to the deformation of the fluid. The greater the value of P', the more "difficult" it is to deform the fluid in order for a density wave to grow and propagate.) If a linear closure for pressure is used, P' is unchanged with increasing density and the bed becomes progressively more unstable as the density increases. If the nonlinear closure for pressure as given in Eq. 22 is used, P' will increase with density ($P' \to \infty$ as $\rho \to \rho_{cp}$). Thus, there will be competition between the stabilizing effect of P' and the destabilizing effect of inertia. The low density instability will occur as before with inertia dominating. However, at high enough densities, the P' value will always dominate over the inertial terms leading to the base state becoming stable with a further increase in density. We have varied the viscosity and the mean density over two orders of magnitude, and, for all the cases we have examined, the same trends as those discussed above were seen.

In the linear stability analysis with the two-phase model, it was seen that there is an intermediate value of the density (between zero and the density at close packing) beyond which the bed is always stable (Anderson et al., 1995). In contrast, no such value is observed with the single-phase model (with the nonlinear closure). This is a result of the fact that the nonlinear closure always predicts values of F_o' that are greater than g and, as was discussed above, the bed is always unstable if this is the case. Therefore, within the framework of the model, it appears that the changing slip velocity between the phases plays an important role in stabilizing the bed at high densities.

Nonlinear Evolution of Plane Waves

The linear stability analysis showed the occurrence of a Hopf bifurcation (at the critical wave number) indicating the birth of a new branch of periodic solutions. It is of interest to examine these solutions taking into account nonlinear terms. The model equations were solved assuming periodic boundary conditions, and the average density of the system was fixed at the density at the uniform state. Since the instability is a traveling wave, the two variables x and t are not independent; therefore, the equations can be transformed by the introduction of a new variable $X = x - ct$. This is equivalent to changing the frame of reference of the observer such that the observer is moving at a speed of c in the positive x direction. In this way the partial differential Eqs. 15 and 16 are transformed into ordinary differential equations.

The continuity equation can then be expressed as

$$\frac{d[\,\rho(v-c)]}{dX} = 0 \tag{26}$$

which implies that $\rho(v-c) = J$ where J is a constant. Since this equation represents an identity, J can be expressed in terms of the values of the variables at the steady state, that is, $J = -\rho_o c$. Then, v, dv/dX and d^2v/dX^2 can be expressed in terms of ρ. The equations of motion (Eqs. 15 and 16) can thus be rewritten solely in terms of ρ and $d\rho/dX$.

The model is thus reduced to a single second order, nonlinear ordinary differential equation of the form

$$\frac{d^2\rho}{dX^2} = \frac{-3\rho^2}{4\mu c\rho_o}[F - \rho g] + \frac{3}{4\mu}\frac{d\rho}{dX}\left[\frac{P'\rho^2}{c\rho_o} - c\rho_o\right] + \frac{2}{\rho}\left[\frac{d\rho}{dX}\right]^2 \tag{27}$$

To solve this equation, expressions for the density dependent force and the fluid pressure are needed and, once again, we will first consider the simplest possible forms, that is, linearly varying functions of density (as described earlier) with parameters listed in Table 1. In particular, the value of F_o' was set to 1.5 g which corresponds to the linear stability results shown in curve III in Figure 2. The nonuniform solutions of the ordinary differential equation were computed by carrying

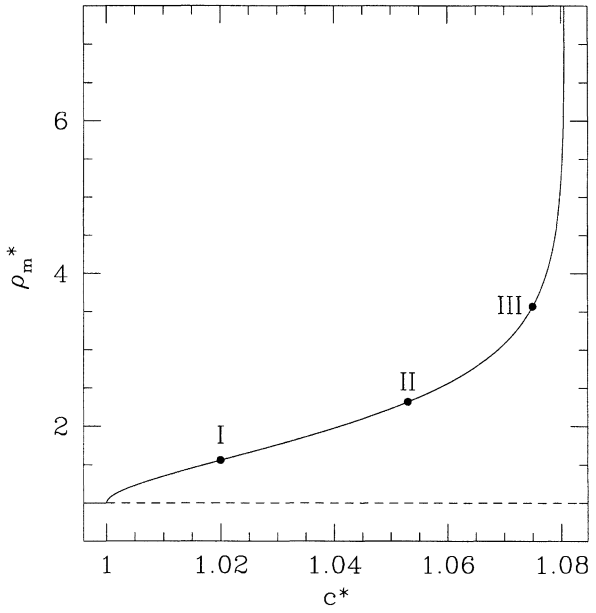

Figure 5. Solutions obtained with linear closures.

Maximum solids density as a function of the wave speed.

out a numerical continuation-bifurcation procedure using AUTO (Doedel et al., 1991). The nonuniform states were found as limit cycles (or periodic orbits) in the variable X. The numerical procedure was checked for accuracy and convergence by verifying that the waves at low amplitudes agree in structure and form with the eigenfunction corresponding to the unstable eigenvalue from the linear stability analysis. The results of the bifurcation analysis are shown in a bifurcation diagram (see Figure 5). In the bifurcation diagram the maximum value of the density wave was plotted as a function of the wave velocity. The wave speed has been nondimensionalized using the velocity at the Hopf bifurcation point for this set of parameters (see Table 1). Note that the values shown for the maximum value (or amplitude) of the solution have been scaled through division by ρ_o, that is, $\rho_m^* = \rho_m/\rho_o$.

In Figure 5, the Hopf bifurcation occurs at $c^* = 1$ as a result of the scaling described above. Every point on this new branch corresponds to a fully-developed traveling wave solution (which can be viewed as a steady-state solution in a frame of reference moving with the wave). The new branch bifurcates supercritically, and there is a gradual increase in amplitude of the waves as c^* increases from 1. It is significant though that this interval of gradual increase is rather small and the amplitude increases extremely rapidly after $c^* = 1.08$.

Representative density profiles were plotted in order to examine the change in the structure of the traveling wave solutions as the wave speed changes. Figure 6a shows the density of the bed as a function of X^o at three different values of the wave speed corresponding to points I, II and III in Figure 5, where $X^o = \alpha X/L$ and $\alpha = -\,sgn\,(c_b)$. The variable α takes on values of plus or minus one and for the current set of parameters, $\alpha = 1$; thus, at this point, it has no effect on the scaling. The variable X^o represents the dimensionless height which is obtained through division of X by the spatial period L corresponding to each wave (and scaled by negative one times the sign of the velocity at the bifurcation). As discussed

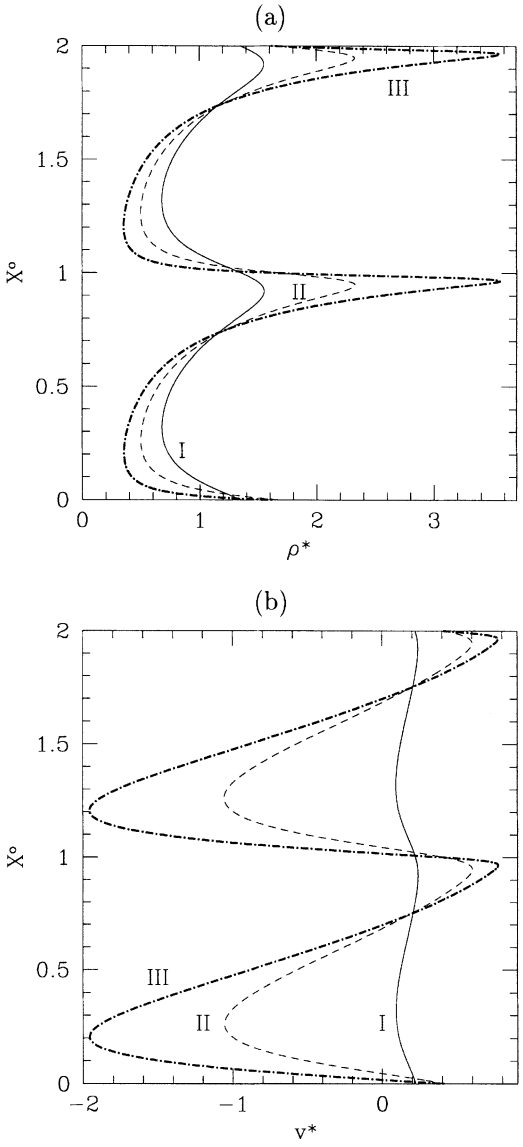

Figure 6. Solutions obtained with linear closures.

(a) Plane traveling waves at various values of the wave speed. The density as a function of X^o. The waves shown correspond to points I, II, and III in Figure 5. (b) Velocity profiles of the plane traveling waves at various values of the wave speed. The waves shown correspond to points I, II, and III in Figure 5. I: $c^* = 1.020$; $L^* = 11.59$; II: $c^* = 1.053$; $L^* = 13.28$; III: $c^* = 1.075$; $L^* = 16.40$.

later in this section, the scaling by α will be useful in accounting for the direction of propagation of the wave. The waves have been plotted over two spatial periods for purposes of clarity. The values of the dimensionless periods L^* are given in the caption (where the period has been made dimensionless through division by the lengthscale, c_b^2/g). Close to the bifurcation point (which occurs at $c^* = 1.0$), the traveling waves are sinusoidal in shape (see Figure 6a, curve I). As the wave speed increases, the fully-developed waves increase in amplitude and get increasingly asymmetrical until they consist of localized regions of high density surrounded by fairly flat regions of low density (see Figure 6a, curves II and III). Since the average density of the system is restricted to a

constant (equal to ρ_o), an increase in the amplitude of the localized high density region is compensated by an increase in the length of the fairly flat region. Traveling waves at high amplitude (as in curve III) have the characteristic density profile of 1-D "clusters" in fluidized beds, that is, localized regions of greater than average density surrounded by fairly flat regions of low density (Glasser et al., 1998).

It should be noted that the spatial period of the traveling waves increases with the wave speed. It is also worth noting that the dimensional wavelengths and wave speeds that are seen here (that is, velocities of the order of 10–100 cm/s and wavelengths of the order of 1–50 cm) are comparable in magnitude to experimentally observed values for bubbles in beds of large diameter (Kunii and Levenspiel, 1991). In order to confirm that the solution structure was robust, the equations were solved for a range of different densities (corresponding to changes over two orders of magnitude) and the same qualitative solution structure (discussed above) was observed for all of the cases considered.

In Figure 6b graphs of the velocity, v^* vs. X^o are shown for points on the bifurcation diagram corresponding to the density profiles in Figure 6a. The velocities are presented in the laboratory frame of reference. The value of the solids velocity at any given value of X can be calculated based on the equation of continuity (Eq. 26). As would be expected from the trend seen in the density, the velocity profiles undergo a gradual transformation from a sinusoidal shape to an asymmetrical shape as the wave speed is increased. However, the degree of asymmetry observed in velocity profiles is less than that observed in the corresponding density profile.

It is clear from these figures that the maximum (and minimum) density corresponds to the maximum (and minimum) velocity. This can be understood from the equation of continuity which requires that, for a given traveling wave, the product of the velocity and the density remain a constant. In particular one can manipulate the equation of continuity to show that for a fully-developed wave with velocity c and average density ρ_o the velocity of the solids in the laboratory frame is given by: $v = c(1 - \rho_o/\rho)$ (Needham and Merkin, 1986). Relative to a laboratory frame of reference, the velocity of the fluid is both positive and negative as the wave passes an observer. The positive velocities correspond to the high density regions, and the negative velocities correspond to the low density regions. This occurs as the flux of fluid over a periodic cell is zero (in the laboratory frame) so any decrease in density in a particular region must be accompanied by fluid flowing from this region (to keep the average flux zero). In a frame of reference moving with the wave, the velocities are all negative (and in the opposite direction to c). This is exactly analogous to the behavior of the solids in a slugging fluidized bed. In a slugging fluidized bed, the flux of solids (in the laboratory frame of reference) is zero and the transfer of solids from a solids rich band to its neighbor below leads to the upwards motion of a slug in a narrow fluidized bed (see Jackson, 2000). However, there is an important difference between the wave forms shown in Figure 6a and the characteristic density profiles of slugs in fluidized beds. In particular, the high amplitude wave forms in Figure 6a represent a localized high density region surrounded by a fairly flat region of low density which is the exact opposite of slugs in fluidized beds (which correspond to a localized region of low density surrounded by a fairly flat region of high density). However, we will show that the equations for a fluid of variable density are capable of capturing solutions that approach slug-like profiles (in addition to the cluster-like solutions which have been described above).

Next, the effect of changing the parameter F_o' to a value less than g was examined. The value of F_o' was set equal to 0.5 g and the other parameters were set to values as listed in Table 1. The bifurcation diagram obtained in this case is identical to Figure 5 (which was generated using a F_o' value of 1.5 g) except for the direction of propagation of the waves. This is consistent with the results from the linear stability analysis described earlier, which indicate that the parameter governing the stability of the bed is in fact $|F_o' - g|$ and that a value of F_o' equal to 0.5 g results in upward propagating waves. This leads to a critical value of the wave speed that is positive (for these parameters, the critical wave speed is 0.173 m/s). The change in the sign of the wave speed at the bifurcation leads to a density profile as a function of X (at any given value of c^*) which is the mirror image of that seen in Figure 6a. However, the fact that the variable X^o is normalized by negative one times the sign of c_b results in the same traveling waves that are shown in Figure 6a, that is, the "flip" in structure of the wave is accounted for by the scaling.

Having considered the simplest case, we have gone on to consider more "realistic" closures (for a fluidized bed) by considering nonlinear forms of closures, as described by Eqs. 22 and 20. This has allowed us to ascertain the sensitivity of the results to changes in the closures. We first considered the nonlinear closure for F in combination with a linear closure for P (Eq. 18). The values of the parameters needed for the nonlinear closure for F were among those given in the first column of Table 2. These parameters were chosen to represent 100 micron glass beads fluidized in air. The value of E used in the linear closure for P is as given in Table 1. It was seen that the evolution of the density profiles is qualitatively the same as described previously for the linear closure for F, that is, the waves are sinusoidal in shape at low amplitudes and they become increasingly asymmetrical as the amplitude increases. With the nonlinear closure for F, the model always captures downward propagating waves. This is because the gradient of F in this case can be reduced to the form

$$F_o' = \frac{u_o g}{v_t(1-(\rho_o/\rho_s))}\left[1 - \frac{\rho_o(1-n)}{1-\rho_o/\rho_s}\right] \qquad (28)$$

and since $(1-n)$ is always a negative number (as $n > 1$), F_o' is always greater than g. We therefore see the characteristic sharp floor, gentle roof slug profile associated with downward propagating waves. This result indicates that realistic values of F_o' are greater than g.

The explanation for this is that the model we have considered consists of the solids equations (in the two phase sense), and the direction of propagation predicted by the linear stability analysis pertains to the solids wave. Through visual observation of a slugging bed, it is expected that the solids wave will be a sedimentation (and, therefore, downward propagating) one. In order to support this scenario and better understand the physical meaning of the direction of propagation of the two phases, we will now return to the two phase model.

Using this approach, we will show that the gas will propagate in the opposite direction of the solids. Consider the result of adding the equations of continuity for the solid and gas phases (Eqs. 1 and 2)

$$\nabla\cdot(\phi \boldsymbol{u}_s) + \nabla\cdot\left[(1-\phi)\boldsymbol{u}_g\right] = 0 \tag{29}$$

If we consider only the vertical direction and integrate with respect to x we can write

$$\phi u_s + (1-\phi)u_g = G \tag{30}$$

where u_g and u_s are the gas and solids velocity, respectively, in the x-direction and the x-subscript has been dropped for convenience. G is a constant which may be solved for in terms of the variables at steady state. We can define G as

$$G = (1-\phi_o)u_o \tag{31}$$

where u_o is the fluidization velocity. The value of u_o may be computed using the steady-state condition (see Eq. 10). Solving explicitly for the gas velocity and substituting in for G we obtain

$$u_g = \frac{(1-\phi_o)u_o - \phi u_s}{(1-\phi)} \tag{32}$$

As discussed earlier in this section, in the case of $F_o' > g$ we have observed that $u_s\ (=v)$ is always negative in the wave frame. If we assume that this solid velocity corresponds to a solids velocity in the two-phase sense, then, since ϕ, ϕ_o, and u_o are positive numbers, the equation above would predict that the gas propagates upwards in this case. An upward propagating solids wave, therefore, requires the physically unintuitive scenario whereby the gas propagates downward through the bed. It therefore seems reasonable that the case of the downward propagating solids wave is the one that results in the profile that is seen with the two-phase model.

In order to ascertain the effect of changes in the closure for P we repeated our calculation using the nonlinear closure for P in Eq. 22. This closure restricts the density to lie below some maximum value ρ_{cp} (which corresponds to the density at close packing). This restriction was not present in the solutions computed using the linear closure of P where the maximum density of the traveling waves could in principle grow without bound. The linear closure for P leads to a gradient in pressure with density $P'(=dP/d\rho)$, which is a constant. This closure was examined because of its simplicity, but it leads to unrealistically large values of ρ for a fluidized bed. In contrast the nonlinear closure for P leads to a gradient in pressure with density, which diverges at ρ_{cp} and thus sets a limit on the value of ρ. Figure 7a shows the bifurcation diagram obtained using the nonlinear closure for both F and P, as described in Eqs. 20 and 22 and the parameters listed in the first column of Table 2. The ρ_o value was chosen to be 1,100 kg/m^3 which is the same, as in Figure 5. The new branch bifurcates supercritically and there is a gradual increase in amplitude as c^* increases from 1.

Figure 7b shows traveling waves corresponding to points I through III in Figure 7a. These represent fully-developed

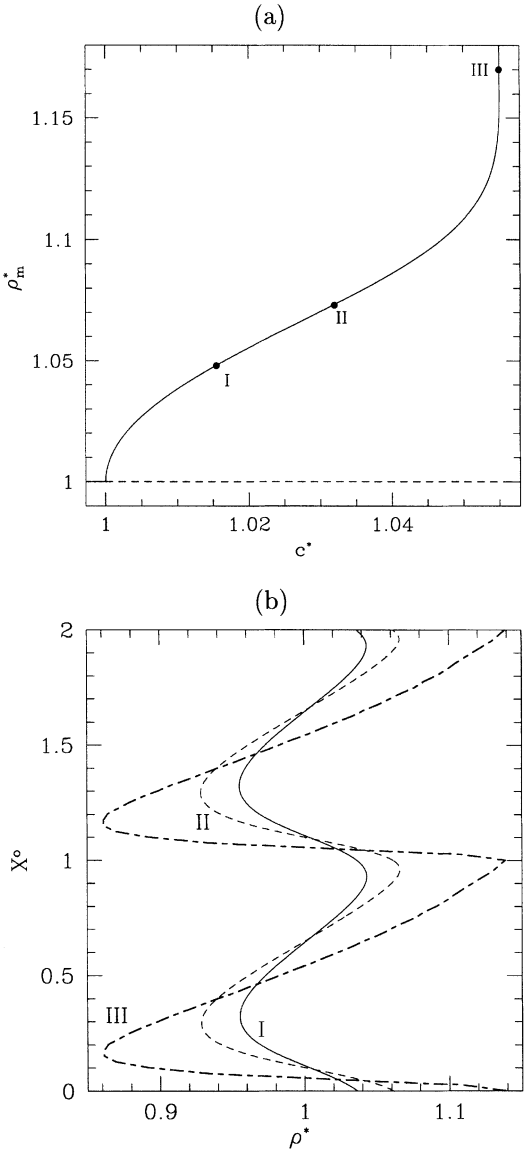

Figure 7. Solutions obtained with nonlinear closures for *F* and *P*.

(a) Bifurcation diagram for plane traveling waves. Maximum solids density as a function of the wave speed. (b) Traveling waves obtained at various values of the wave speed. The density as a function of X^o. The waves shown correspond to points I, II, and III in part (a). (I) $c^* = 1.015$; $L^* = 1.330$; (II) $c^* = 1.032$; $L^* = 1.453$; (III) $c^* = 1.055$; $L^* = 2.946$.

waves at increasingly higher wave speeds, and it can be seen that the density profiles evolve from a sinusoidal shape to a highly asymmetrical one as the wave speed is increased. The maximum density is limited to the density at close packing (which would occur in this case at a ρ^* value of 1.3). However, as the maximum density in the waves approaches this limit, the waves approach nearly vertical wave fronts (see curve III) and the numerical continuation scheme we have adopted is not able to follow the branch any appreciable distance beyond this point.

The profiles at the highest amplitude in Figure 7a appear qualitatively different from those in Figure 5 (see Figure 6a for the corresponding density profiles). In Figure 5 the high-

est amplitude waves are characterized by a nearly flat region of low density (that approaches a ρ^* of zero) surrounded by a localized region of high density (where the maximum density, ρ_m^* is not limited to any particular value). However, the same cannot occur once the nonlinear closure for P is used, as the maximum in density cannot exceed a pre-determined value (which equals the density at close-packing). As shown in Figure 7b, at high wave speeds, an increase in the amplitude of the bed is manifested primarily by decreases in the minimum density (and by small increases in ρ_m^*). Based on limitations of the numerical scheme used to compute these traveling waves, we have not been able to follow the traveling waves as ρ_m values approach ρ_{cp} (since the wave fronts become nearly vertical before this point). However, based on the profiles shown, we would expect that once the traveling waves achieve a maximum density that approaches ρ_{cp}, further increases in the amplitude of the wave would be manifested by flat regions close to the ρ_{cp} value, compensated by progressively lower values of the minimum density. However, it should be noted that the slug-like solutions are not captured as well as they are with the two-phase model (Glasser et al., 1998). This suggests that a nonconstant slip velocity is important in this case. This highlights one of the limitations of the simplified model.

Figure 8 shows the results obtained when the density at the uniform state is decreased (again, with the nonlinear form for both closures). Note that the scalings used in this figure are those corresponding to the value of ρ_o (given in the caption) for this case. Figure 8a shows the bifurcation diagram obtained in a dilute bed using the nonlinear closures for F and P. It can be seen that the uniform state evolves such that fairly high values of maximum density are achieved. Three representative traveling wave solutions are shown in Figure 8b, and it can be seen that the shape of the instability evolves from a sinusoidal shape to a cluster-like solution (localized regions of high density in an otherwise dilute bed). As curve III in Figure 7b shows, the traveling waves in dense beds evolve into "slug-like" shapes (localized regions of lower than average density in an otherwise dense bed) at densities near close-packing. As discussed above, although the trend from cluster to slug-like solutions is captured by the model, the slug-like solutions cannot be followed to very high amplitudes. However, we believe this is a numerical issue and not a deficiency of the model since we have been able to capture slug-like solutions using a different combination of closures than considered above. Figure 9 shows a representative high

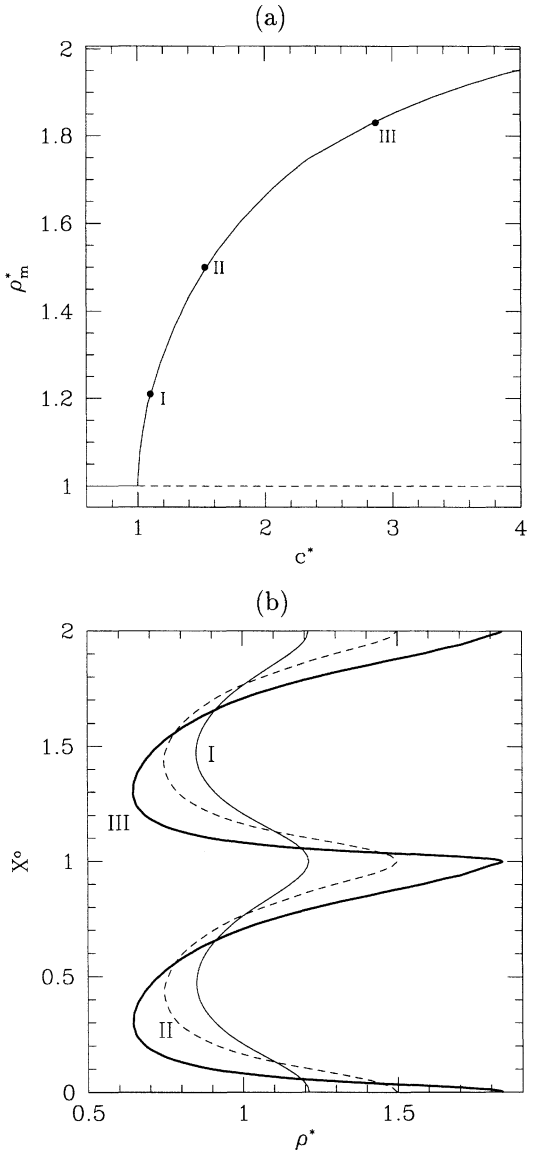

Figure 8. Solutions obtained with nonlinear closures for F and P at $\rho_o = 660$ kg/m^3.

(a) Bifurcation diagram for plane traveling waves. Maximum solids density as a function of the wave speed. (b) Traveling waves obtained at various values of the wave speed. The density as a function of X^o. The waves shown correspond to points I, II, and III in part (a). (I) c* = 1.101; L* = 21.23; (II) c^* = 1.523; L* = 25.85; (III) c^* = 3.518; L* = 37.54.

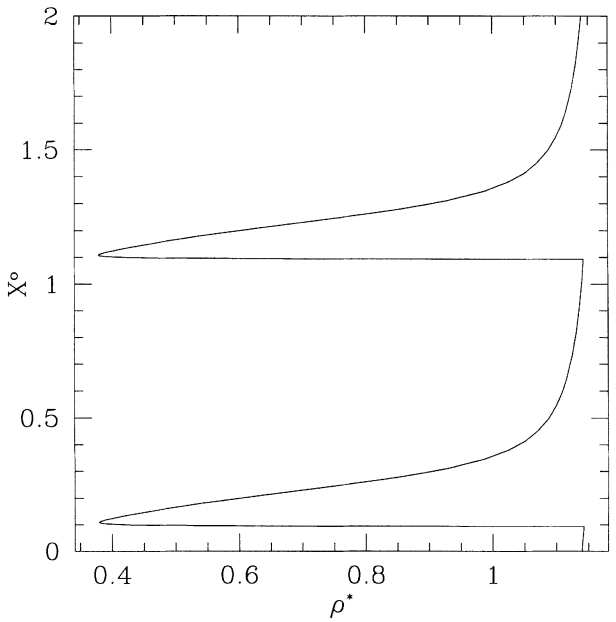

Figure 9. Representative traveling wave at $\rho_o = 1{,}210$ kg/m^3 with a nonlinear form of P and a linear form of F.

The density as a function of X^o. c^* = 1.033; L* = 45.15.

amplitude solution obtained in a dense bed when the nonlinear closure for P is used in conjunction with the linear closure for F. The relevant parameters from Table 1 are used. In this case, the solution resembles a slug as shown by the flat regions of nearly uniform density.

It can be seen that the form of the closures affects the shapes of the solutions, the direction of propagation and the sub/supercritical behavior of the instability of the compressible fluid. However, in all cases the uniform state loses stability at a Hopf bifurcation and a branch of plane traveling waves is born. In the next section we will evaluate the stability of the plane waves in the lateral direction.

Instability of the Plane Waves

The stability of the plane waves to 2-D perturbations can be used to shed light on the development of lateral structure in such waves. The development of transverse structure for the plane waves was examined by considering the partial differential equations describing the fluid of variable density (see Eqs. 13 and 14) in two dimensions. This was accomplished using a pseudo-spectral discretization scheme with Fourier basis functions (see Canuto et al. (1988) for a description of the algorithm and its convergence properties and Brown (1992) for its application to traveling waves). We have considered the stability of the plane waves to perturbations which are periodic in the lateral direction and have the same vertical periodicity as the plane waves themselves. The stability analysis was carried out by approximating the variables ρ, v_x, and v_y with a Fourier series. As before, we will examine the traveling wave in a frame of reference moving with the wave by defining the variable $X = x - ct$. We will thus compute the plane waves as steady solutions in this coordinate system and evaluate their stability to 2-D perturbations.

Any variable ψ that is periodic in both X and y can be approximated in terms of the vertical wave number (κ) and the lateral wave number (λ) as follows

$$\psi^{\theta}_{N,M} = \sum_{m=0}^{M} \left[b^{\theta}_{0,m}(t) + \sum_{n=1}^{N} \left\{ a^{\theta}_{n,m}(t) \sin(nX\kappa) + b^{\theta}_{n,m}(t) \cos(nX\kappa) \right\} \frac{1}{2} \right] \cos(my\lambda) + \sum_{m=1}^{M} \times \left[d^{\theta}_{0,m}(t) + \sum_{n=1}^{N} \left\{ c^{\theta}_{n,m}(t) \sin(nX\kappa) + d^{\theta}_{n,m}(t) \cos(nX\kappa) \right\} \right] \sin(my\lambda) \quad (33)$$

The density and the two components of the velocity were approximated with the Fourier expansion above and substituted into the model equations. In the following analysis, we have neglected oblique traveling waves by discarding the second group of terms in the approximation of density and the velocity in the vertical direction. For the velocity in the lateral direction, the first group of terms is neglected for the same reason. The inner product of the resulting equations was evaluated using the inverse Fourier transform. The results were computed in the traveling wave frame by explicitly solving for the wave speed as part of the solution.

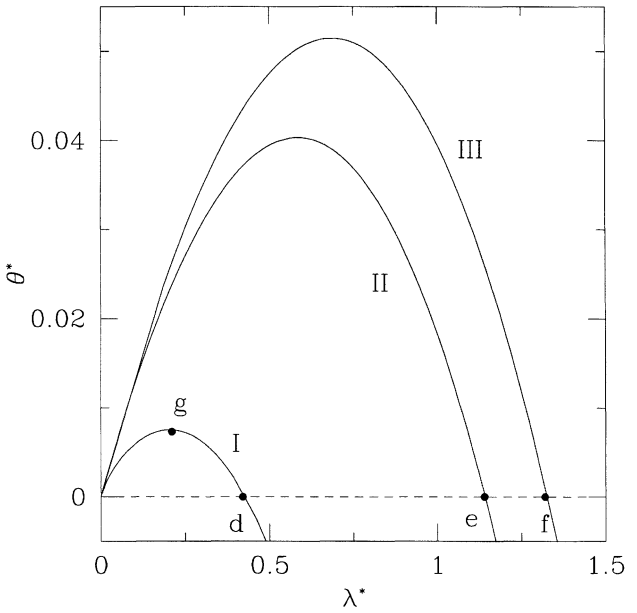

Figure 10. Nonlinear stability analysis of the plane waves.

The corresponding plane waves are shown in Figure 7b. (I) $\kappa^* = 4.93$; (II) $\kappa^* = 4.72$; (III) $\kappa^* = 4.33$.

The stability of the 1-D solutions was studied by varying the lateral wave number λ of the disturbances (or width of the periodic box in the horizontal direction). Figure 10 shows the dimensionless growth rate θ^* of the 2-D disturbances, plotted vs. the dimensionless lateral wave number λ^* for various plane waves corresponding to Figure 7b. The lateral wave number and growth rate have been nondimensionalized using the scalings c_b^2/g and $|c_b|/g$, respectively. The vertical wave numbers κ^* corresponding to the plane waves are listed in the caption (where $\kappa^* = 2\pi/L^*$). The parameters are listed in the first column of Table 2 and the closures are given by Eqs. 22 and 20. Curve I in Figure 10 corresponds to point I in Figure 7a and the plane wave shown as curve I in Figure 7b. It can be seen that the wave is stable for large λ^*. As λ^* is decreased, the plane wave loses stability and one real eigenvalue passes through zero (in the wave frame). This represents a pitchfork bifurcation in the wave frame. As λ^* is further decreased, the growth rate goes through a maximum and finally decreases to zero as λ^* tends to zero. Curves II and III correspond to points II and III, respectively, in Figure 7a and the plane waves shown as curves II and III in Figure 7b. It can be observed that as the amplitude of the plane waves is increased, the waves lose stability at progressively larger lateral wave numbers. In other words, the higher the amplitude of a given plane wave, the larger the range of lateral wave numbers for which it is unstable. In each case the loss of stability is associated with one real eigenvalue going through zero.

Next, we examine the eigenfunctions corresponding to the transverse instability. Figure 11 shows the eigenfunction at the critical stability point (that is, point d) on curve I in Figure 10. The corresponding plane wave is shown in Figure 11a. The eigenfunctions associated with the density and fluid velocity are shown in Figure 11b and Figure 11c, respectively.

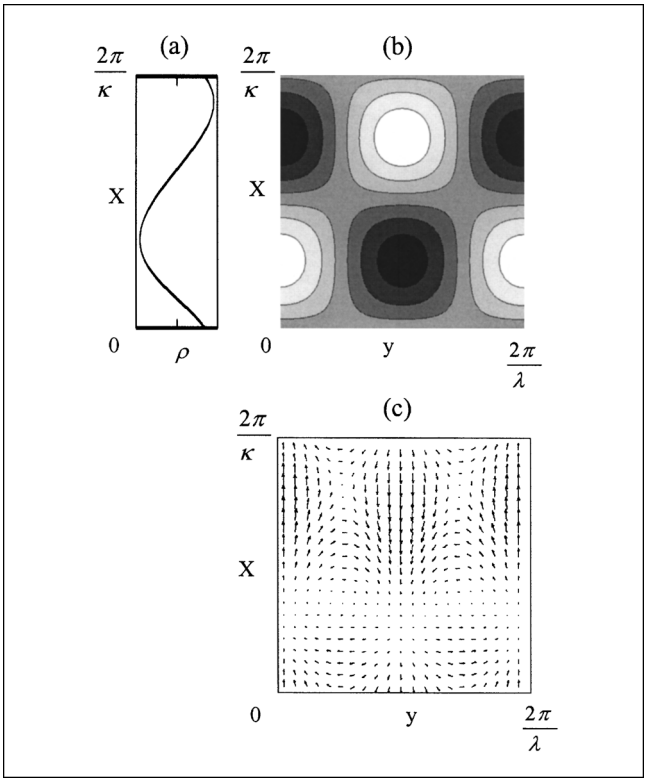

Figure 11. Stability analysis in the lateral direction for $\kappa^* = 4.93$, $\lambda^* = 0.423$ (or point I in Figure 7a), $N = 4$ and $M = 1$.

(a) Corresponding plane wave, ρ vs. X (see Figure 7b for quantitative information); (b) eigenfunction associated with the density; (c) eigenfunction associated with the fluid velocity.

Figures 11b and 11c are plotted over one period of height $2\pi/\kappa$ and width $2\pi/\lambda$ using N vertical and M lateral modes (the values of which are given in the caption). The eigenfunctions are plotted in a square box for clarity even though the ratio of the vertical to lateral wave numbers is not unity. For low amplitude plane waves, the eigenfunction associated with the density is approximately sinusoidal in the vertical direction with a superimposed mode in the lateral direction. The eigenfunction associated with the fluid velocity shows a recirculation loop with the vertical component of the velocity dominating the lateral component. In accordance with the lateral symmetry of the density related eigenfunction, the fluid velocity of the perturbation mirrors itself every half wavelength in the vertical direction.

We have seen a gradual change in the density-related eigenfunctions as the amplitude of the plane wave is increased. Starting from a vertical form that is approximately sinusoidal, the eigenfunction begins to get progressively more asymmetrical in the vertical direction as the plane waves change in form in an analogous manner. The net effect is to confine the largest variations in the density perturbation into progressively smaller areas. Note that this change is reflected in the plane waves where the variation in density tends to get increasingly localized at lower wave numbers. In addition, the lateral component of the solids velocity becomes increasingly larger as the vertical wave numbers of the plane waves decrease until the lateral component begins to dominate the vertical component. We have examined a large number of plane waves and observed the same behavior for the transverse instability for all the cases considered.

The eigenfunctions corresponding to the loss of stability in the lateral direction show the same basic structure as those observed using the two-phase model (Glasser et al., 1996). In particular, the density eigenfunctions corresponding to low amplitude waves display a cellular structure that is indistinguishable for the simplified and two-phase models. This leads us to conclude that the mechanism by which 2-D structure develops in fluidized beds is captured by the compressible flow equations. Moreover, this work ties in directly with the overturning instability observed by Batchelor and Nitsche (1991) for a stratified fluid and by Batchelor (1993) for a particle dispersion with a sinusoidal variation in density. The plane waves predicted by the model presented here take a sinusoidal form at low amplitudes and the density and velocity eigenfunctions share the same basic cellular structure as those computed by Batchelor and Nitsche (1991). In particular we observe the alternating columns of fluid moving in opposite directions every half wavelength that are characteristic of the "overturning" instability (Batchelor and Nitsche, 1991; Batchelor, 1993). Moreover, we have observed that even for waves with rather sharp profiles where the nonlinear terms become important, the basic structure of the instability is preserved.

Further parallels may be drawn between the results of the current work and the two-phase model for fluidized beds. We have seen that the transverse instability is a long wave instability whereby any given plane wave will be unstable in a wide enough bed. This finding is in accordance with the stability analyses of Göz (1995) and Göz and Sundaresan (1998) for fluidized beds where they discerned that the plane wave becomes unstable at arbitrarily small amplitudes for a wide enough bed. We have also observed that, as the amplitude of the plane waves increases, the waves lose stability at progressively larger lateral wave numbers, which agrees with the scaling results of Göz (1995). Finally, it should be noted that Didwania and Homsy (1982) investigated a secondary instability in a fluidized bed and observed that a transverse structure can develop due to a weakly nonlinear resonant sideband instability. The possibility of such an instability occurring in the plane waves that we have observed has not been investigated and can certainly not be ruled out as a route to the formation of transverse structure.

Discussion

Drag (for the Reynolds numbers of interest here) consists of a function of solids fraction multiplied by the relative velocity of the two phases. Therefore, an increase in drag can be due to an increase in solids fraction or an increase in the relative velocity of the two phases. We have shown that it is sufficient to have a function which only varies with solids fraction to observe the primary instability of the uniform state and the secondary instability of this plane wave. Such a form for drag can be obtained by taking the zeroth-order term for a Taylor series of the slip velocity about the uniform state. We will now examine whether this simplification is physically valid using the two-phase model, as described by Eqs. 1–4.

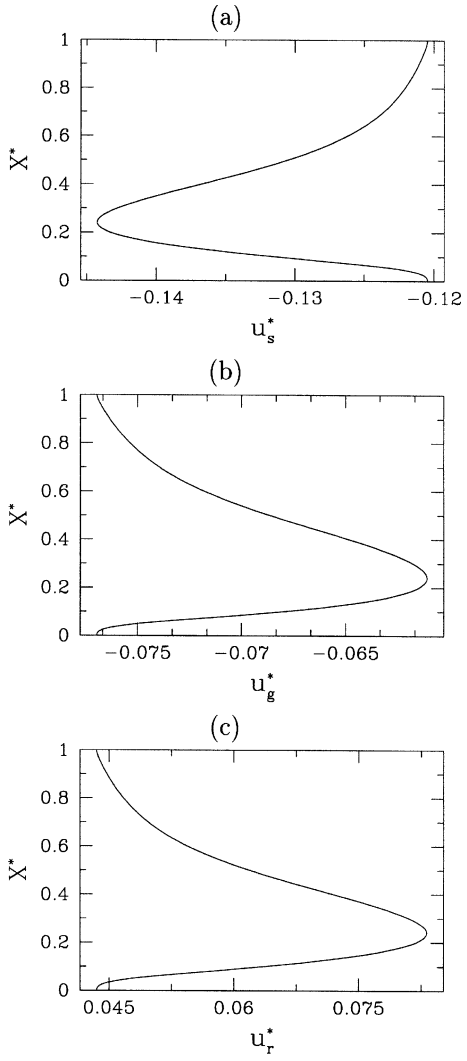

Figure 12. Velocity as a function of height for 200 micron glass beads fluidized in air.

Velocities computed using the two-phase model and the parameters listed in column 2 of Table 2. $\hat{\kappa} = 35.95$. (a) Solid velocity u_s^*; (b) gas velocity u_g^*; (c) relative velocity, u_r^*.

The two-phase model was used to examine typical profiles of the relative velocity between the gas and solid phases. The nonlinear closures as given in Eqs. 20 and 22 were used in conjunction with a constant value of the viscosity to solve for the 1-D traveling wave solutions. The list of the parameter values used in this case appears in the second column of Table 2 and represents 200 micron glass beads fluidized in air. The Fourier series approximation and pseudo-spectral discretization scheme that was described in the previous section was used to carry out the bifurcation analysis and continuation on the two-phase model.

Representative profiles of the solids velocity, gas velocity and the relative velocity (in a frame of reference moving with the wave) are presented in Figures 12a, 12b and 12c, respectively. Note that all the velocities in this case have been scaled through division by the terminal velocity of a particle v_t while X has been made dimensionless through division by the spatial period, that is, $X^* = X/L$. The value of the vertical wave number $\hat{\kappa}$ is given in the caption, where κ has been made dimensionless through multiplication by v_t^2/g. It can be seen that the largest (smallest) gas velocity corresponds to the smallest (largest) solids velocity. Thus, there is a tendency for an increase in the solids velocity to be compensated for by a decrease in the gas velocity. It can be seen that the relative velocity (shown in Figure 12c) is not a constant in X^*. Therefore, the fact that the richness of the two-phase model is retained under the assumption of constant relative velocity is remarkable. This ability of the single-phase model to capture the salient features of the two-phase model may be better understood by examining the contributions of several relevant terms to the Taylor series of the drag force.

Note that in the following analysis, we will only consider the vertical components of the fluid and solids velocities. Consider the first order Taylor series expansion of $\hat{F} = \beta(u_g - u_s) = \beta u_r$

$$\hat{F} = \beta_o u_o + \left.\frac{\partial(\beta u_r)}{\partial x}\right|_{x_o} (x - x_o) \tag{34}$$

To obtain the expression above, $\hat{F}$ is linearized about a point x_o where the value of ρ is equal to ρ_o and the value of the relative velocity is equal to u_o. Because the phase of the wave is arbitrary, the actual value of x_o is arbitrary. Thus without any loss of generality, we take x_o equal to zero.

Re-writing u_r as a combination of a constant u_o and a deviation from this value u_r', the expression above can be expanded to obtain

$$\hat{F} = \beta_o u_o + (u_o + u_r')\left.\frac{\partial\beta}{\partial x}\right|_{x_o} (x - x_o) + \beta\left.\frac{\partial u_r'}{\partial x}\right|_{x_o} (x - x_o)$$

If the relative velocity u_r is assumed to be a constant equal to u_o, then we obtain

$$\hat{F} = \beta_o u_o + u_o\left.\frac{\partial\beta}{\partial x}\right|_{x_o} (x - x_o) \tag{35}$$

By comparing Eqs. 34 and 35, it can be seen that the assumption of a constant relative velocity leads to the following approximation

$$\left.\frac{\partial(\beta u_r)}{\partial x}\right|_{x_o} = u_o\left.\frac{\partial\beta}{\partial x}\right|_{x_o}. \tag{36}$$

Therefore, applying our assumption implies neglecting the term δ where

$$\delta = u_r'\left.\frac{\partial\beta}{\partial x}\right|_{x_o} + \beta\left.\frac{\partial u_r'}{\partial x}\right|_{x_o} \tag{37}$$

The replacement of u_r with a constant is therefore reasonable provided we can prove that Eq. 36 is physically sound. We will also demonstrate that neglecting the term δ is justifiable for the purposes of the present model.

The two phase model described by Eqs. 1–4 was used to compute $\partial(\beta u_r)/\partial x|_{x_o}$, $u_o(\partial\beta/\partial x)|_{x_o}$ and δ. Figure 13 shows

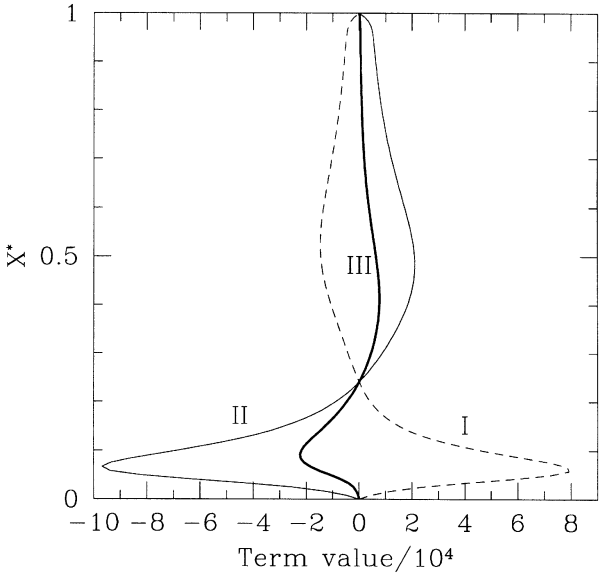

Figure 13. Comparing magnitudes of key quantities in the Taylor series expansion of $\hat{F}$.

See Eqs. 35 and 37 for their definitions. Results obtained using the two-phase model and the parameters given in column 2 of Table 2. (I) δ, (II) $u_o(\partial\beta/\partial x)|_{x_o}$; (III) $[\partial(\beta u_r)/\partial x]|_{x_o}$.

values of $\partial(\beta u_r)/\partial x|_{x_o}$, $u_o(\partial\beta/\partial x)|_{x_o}$ and δ as a function of the dimensionless X value, for the representative traveling wave (shown in Figure 12). Although the magnitudes of $u_o(\partial\beta/\partial x)|_{x_o}$ and δ are relatively similar, it can be seen that they always have the opposite sign relative to each other and $\partial(\beta u_r)/\partial x|_{x_o}$ is the sum of these two quantities. Despite the fact that the variation in $\partial(\beta u_r)/\partial x|_{x_o}$ is much smaller than that in either $u_o(\partial\beta/\partial x)|_{x_o}$ or δ, it should be noted that the sign of $\partial(\beta u_r)/\partial x|_{x_o}$ follows the sign of $u_o(\partial\beta/\partial x)|_{x_o}$. Therefore, the replacement of the relative velocity in the density dependent force with a constant is justifiable for a model aimed at ascertaining qualitatively correct behavior. However from a purely quantitative point of view, such a model would not correctly capture the exact magnitude of the various terms.

An examination of Figure 13 leads one to ask whether retaining only the first term of Eq. 34 is sufficient to capture the basic features of the instability. Such a simplification leads to the case where the density dependent force is given by

$$F = Q \tag{38}$$

where Q is a constant determined by the steady state condition (i.e., $Q = \rho_o g$). This is equivalent to a constant drag coefficient but Q (or F) is not an independent constant as its value is related to the average density. We have considered this closure in conjunction with both linear and nonlinear closures for the solid pressure (see Eqs. 18 and 21). Figure 14 shows the result of the linear stability analysis when Eqs. 38 and 18 were used as the closures for F and P respectively. The parameters (other than the parameter A) are as given in Table 1 and the value of Q is given in the caption of the figure. From Figure 14a, it can be seen that once again the growth rate rises from zero to reach a maximum and then

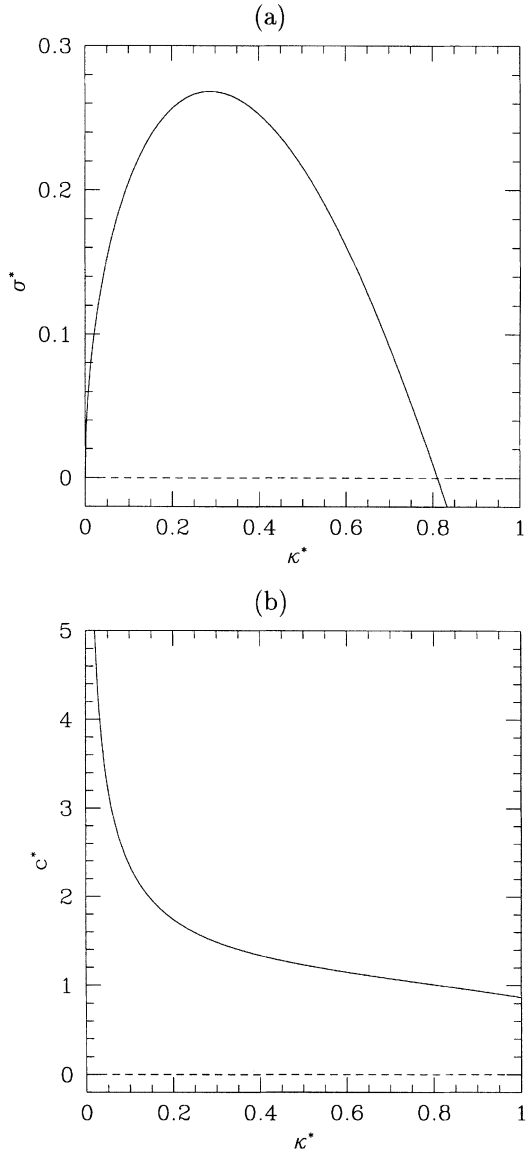

Figure 14. Linear stability analysis using a constant for the density dependent force (see Eq. 38) and a linear closure for P.

$Q = 10{,}780$ kg/(m^{2}s^2). (a) Real part of the growth rate vs. the wave number; (b) phase velocity vs. the wave number.

decreases, going through zero at a Hopf bifurcation. As Figure 14b shows, the wave speed decreases very sharply at low wave numbers and then levels out. Figure 15a shows the bifurcation diagram obtained for this case. It can be seen that the branch bifurcates supercritically and the amplitude increases as c^* increases from 1. The traveling waves corresponding to points I, II and III are shown in Figure 15b. A gradual development from a sinusoidal shape to an increasingly asymmetrical shape is shown. We also examined the above closure for the density dependent force (Eq. 38) together with the nonlinear closure for the particle pressure (Eq. 21). As previously observed for the nonlinear pressure P, the traveling waves gradually developed from a sinusoidal shape to an increasingly asymmetrical shape resembling

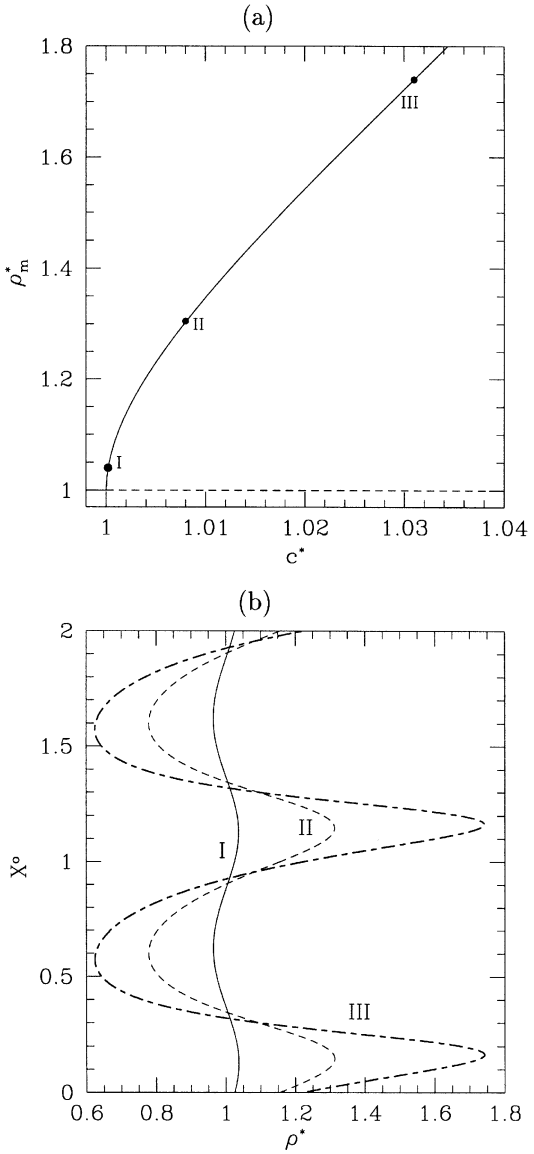

Figure 15. Solutions obtained using a constant for the density dependent force (see Eq. 38) and a linear closure for *P*.

$Q = 10{,}780$ kg/(m^{2}s^2). (a) Bifurcation diagram for plane traveling waves. Maximum solids density as a function of the wave speed. (b) Traveling waves obtained at various values of the wave speed. The density as a function of X^o. (I) $c^* = 1.001$, $L^* = 1.648$; (II) $c^* = 1.008$, $L^* = 3.821$; (III) $c^* = 1.031$, $L^* = 13.74$.

slug-like solutions, and the qualitative features were the same as those discussed earlier.

Thus, in terms of the qualitative features of the instability of a fluidized bed, we have shown that the primary role of the gas is to provide a density dependent force (through drag). A linear stability of the uniform state shows the bed is stabilized by increases in viscosity and the gradient in particle pressure. This analysis highlights the key role of the parameter P'_o which determines the wave speed at which the bifurcation occurs. It was shown that the sign of $(F'_o - g)$ governs the direction of propagation of instability and the magnitude determines the destabilizing effect of the parameter. In addition, density was shown to be potentially stabilizing and destabilizing depending on the value of ρ_o. Bifurcation and continuation showed the occurrence of a Hopf bifurcation which gives rise to traveling wave solutions that develop from a sinusoidal shape to increasingly asymmetrical "cluster-like" shapes. The results of continuation in beds of varying values of ρ_o (in conjunction with nonlinear closures) showed "cluster-like" instabilities evolving into profiles that approach "slug-like" instabilities as the value of ρ_o was increased.

As was discussed, it has been conjectured by Batchelor (1991, 1993) that bubbles originate from an unstable uniform fluidized bed in various stages. The first stage is the primary instability of the uniform state which leads to plane waves. A secondary instability follows which leads to lateral concentration variations. Finally, a compact region of low concentration develops; this compact region rises and particles are expelled from this region (see Batchelor and Nitsche, 1994). From our work, we can conclude that a compressible fluid acted upon by a density dependent force will undergo a primary instability which leads to the formation of plane density waves. These plane density waves in turn will undergo a secondary instability in the transverse direction. These instabilities represent the first two stages of bubble development that were postulated by Batchelor (1991). Although our present analysis does not allow us to definitively answer the question of whether a compact region of low concentration will form, we can use the results of the stability analysis of the plane waves to further examine the solution structure. In particular small disturbances to the plane waves will be governed by linear equations. Therefore, we can examine the structure of solutions on the unstable manifold of the (unstable) plane waves by adding the plane wave solution and the eigenfunction corresponding to the most unstable eigenvalue. In Figure 16 we show the results of such a linear perturbation for the plane wave corresponding to curve I in Figure 7b. (The stability analysis for this wave is shown in Figure 10.) Figure 16a shows the results of adding a small amount of the eigenfunction at point g in Figure 10. The perturbation results in a "buckling" of the plane wave. As shown in Figure 16b, when the plane wave is perturbed even further (by adding a larger amount of the eigenfunction), a cellular structure emerges. This strongly suggests that the compressible fluid model is capable of successfully capturing the process of bubble formation in two dimensions, although a more rigorous analysis of the full 2-D solutions would be necessary to establish the capabilities and limitations of this model.

In general, gas-particle interactions, as well as particle-particle interactions, can lead to the formation of density inhomogeneities in gas-particle flows (Agrawal et al., 2001). In particular it has been shown that clusters can arise from inelastic collisions between particles (Goldhirsch and Zanetti, 1993). The role of inelastic collisions has not been treated in our analysis. However, work on equations of motion for granular materials (Sela and Goldhirsch, 1998) suggests that the effect of inelastic collisions could be incorporated into such an analysis. However, this is beyond the scope of the present contribution, although it is needed in order to develop a complete understanding of density waves in fluidized beds. In particular we would expect that such effects could be quite important in dilute fluidized beds where cluster-like solutions have been observed (Agrawal et al., 2001) and energy dissipa-

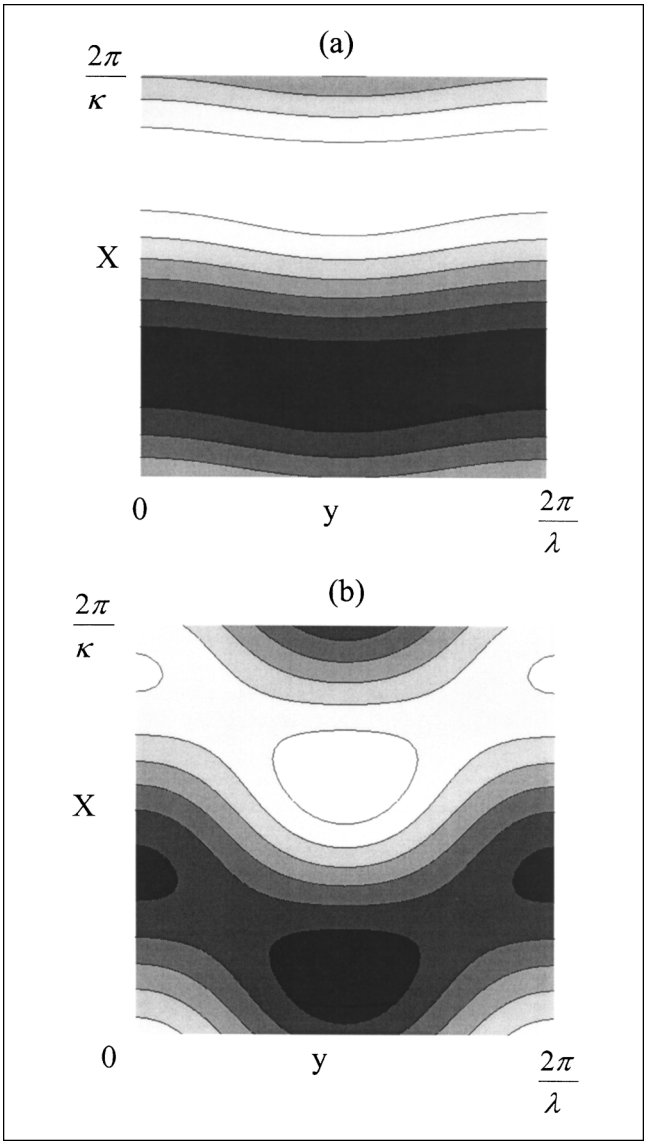

Figure 16. Gray scale plots of density obtained by adding a fraction of the unstable eigenfunction to the plane traveling wave.

$\kappa^* = 4.93$, $\lambda^* = 0.237$. This figure corresponds to point g in Figure 9 and the plane wave seen as curve I in Figure 6b. (a) The "buckling" of the wave when a small fraction of the eigenfunction is added; (b) the emergence of a bulging "bubble-like" solution when a larger fraction of the eigenfunction is added.

tion due to inelastic collisions would be expected to be significant.

Our results have shown that the analogy between a gas-particle flow and a compressible flow can be used to improve our understanding of the flow of gas and particles in a fluidized bed. We have restricted our analysis to the case of gas-fluidized beds where the fluid density is much smaller than that of the solid. However, it may be possible to set up a similar model for liquid-fluidized beds by writing the equations in a form where the inertia of the fluid and solid are combined as the inertia of the suspension (Jackson, 1994). In addition, general multiphase momentum equations for two phases often resemble the Navier-Stokes equations with an interaction term between the two phases. The interaction forces can arise from a variety of physical mechanisms, but these forces often share some common themes. Some examples of such flows are bubbly gas-liquid flows, trickle-bed flows (flow of gas and liquid through a packed bed), and gas-particle flows. In many cases the interaction forces can be written in a form which varies with the volume fraction occupied by the different phases. In fact, in some of these systems the assumption of a constant slip velocity between the two phases concerned may be quantitatively justifiable (Sokolichin and Eigenberger, 1999). That would make this approach an even better candidate for exploration. A homogeneous or base state exists in all the above-mentioned examples and this base state can lose stability in the form of voidage waves such as pulsing in trickle beds (Blok, Varkevisser, and Drinkenburg, 1983; Dankworth, Kevrekidis, and Sundaresan, 1990) and bubbly flows (Becker et al., 1994). The common experimentally observed instabilities and common form for the equations of motions leads us to conjecture that the same essential physics may be taking part in the instability of the base state and the development of voidage waves in all of these flows. In order to fully understand the relationship between wave forms in compressible flows, gas-liquid flows, and gas-particle flows, further work on wave hierarchies in all these flows is needed.

We have shown that the qualitative features of the primary and secondary instability of a fluidized bed can be captured by the compressible flow equations with a density-dependent force. The choice of closures does not change the nature of the instabilities, but does change the quantitative features of the solutions. However, the ability of the model equations to capture slug-like solutions in dense beds is compromised by the assumption of a constant relative velocity. Instabilities in dilute beds are, however, captured well. This suggests that the formation of slugs is critically dependent on the acceleration or deceleration of the particles relative to the fluid. In general, this work supports the idea that the occurrence of bubble-like or cluster-like solutions in a simulation of a fluidized bed does not mean that the "correct" form of the equations of motion have been used or suitable closures have been found. Instead, this work, along with previous work (Göz, 1995; Göz and Sundaresan, 1998), suggests that such voidage waves are generic. At the same time, the closures will affect the detailed structure of the wave forms. In this regard, more work is needed to measure and develop suitable closures for fluidized beds. With suitable closures, the equations describing the flow of gas and particles in a fluidized bed could potentially lead to vast improvements in the design, scale-up, and operation of these units.

Acknowledgment

This work has been partially supported by the National Aeronautics and Space Administration. One of the authors (B.J.G.) would like to thank Professor Roy Jackson for stimulating discussions while at Princeton University, which laid the groundwork for this study.

Literature Cited

Agrawal, K., P. N. Loezos, M. Syamlal, and S. Sundaresan, "The Role of Meso-Scale Structures in Rapid Gas-Solid Flows," *J. Fluid Mech.*, **445**, 151 (2001).

Anderson, T. B., and R. Jackson, "A Fluid Mechanical Description of Fluidized Beds. Equations of Motion," *Indust. Eng. Chem. Fundam.*, **6**, 527 (1967).
Anderson, T. B., and R. Jackson, "A Fluid Mechanical Description of Fluidized Beds. Stability of the State of Uniform Fluidization," *Indust. Eng. Chem. Fundam.*, **7**, 12 (1968).
Anderson, K., S. Sundaresan, and R. Jackson, "Instabilities and the Formation of Bubbles in Fluidized Beds," *J. Fluid Mech.*, **303**, 327 (1995).
Batchelor, G. K., "A New Theory of the Instability of a Uniform Fluidized Bed," *J. Fluid Mech.*, **193**, 75 (1988).
Batchelor, G. K., "The Formation of Bubbles in Fluidized Beds," *Proc. Honoring John W. Miles on his 70th Birthday*, University of California, San Diego, Ref. Ser., San Diego Scripps Institution of Oceanography, Technical Publication Office, University of California, San Diego, 91 (1991).
Batchelor, G. K., "Secondary Instability of a Gas Fluidized Bed," *J. Fluid Mech.*, **257**, 359 (1993).
Batchelor, G. K., and J. M. Nitsche, "Instability of Stationary Unbounded Stratified Fluid," *J. Fluid Mech.*, **227**, 357 (1991).
Batchelor, G. K., and J. M. Nitsche, "Expulsion of Particles from a Buoyant Blob in a Fluidized Bed," *J. Fluid Mech.*, **278**, 63 (1994).
Becker, S., A. Sokolichnin, and G. Eigenberger, "Gas-Liquid Flow in Bubble Columns and Loop Reactors: II. Comparison of Detailed Experiments and Flow Simulations," *Chem. Eng. Sci.*, **49**, 5747 (1994).
Berryman, J. G., "Random Close Packing of Hard Spheres and Disks," *Phys. Rev. A*, **27**, 1053 (1982).
Blok, J. R., J. Varkeviser, and A. A. H. Drinkenburg, "Transition to Pulsing Flow, Holdup and Pressure Drop in Packed Columns with Cocurrent Gas-Liquid Downflow," *Chem. Eng. Sci.*, **38**, 687 (1983).
Bouillard, J. X., and D. Gidaspow, "On the Origin of Bubbles and Geldart's Classification," *Powder Technol.*, **68**, 13 (1991).
Brown, H. S., "A Computer Assisted, Nonlinear Dynamic Study of Instabilities and Pattern Formation for Interfacial Waves," PhD Diss., Princeton University (1992).
Canuto, C., M. Y. Hussaini, A. Quarteroni, and T. A. Zang, *Spectral Methods in Fluid Dynamics*, Springer, New York (1988).
Childress, W. S., and E. A. Spiegel, "Archimedean Instabilities in Two-Phase Flows," *SIAM Rev.*, **17**, 136 (1975).
Dankworth, D. C., I. G. Kevrekidis, and S. Sundaresan, "Dynamics of Pulsing Flow in Trickle Beds," *AIChE J.*, **36**, 605 (1990).
Dasgupta, S., R. Jackson, and S. Sundaresan, "Turbulent Gas-Particle Flow in Vertical Risers," *AIChE J.*, **40**, 215 (1994).
Daw, C. S., C. E. A. Finney, M. Vasudevan, N. A. van Goor, K. Nguyen, D. D. Bruns, E. J. Kostelich, C. Grebogi, E. Ott, and J. A. Yorke, "Self-Organization and Chaos in a Fluidized Bed," *Phys. Rev. Lett.*, **75**, 2308 (1995).
Didwania, A. K., and G. M. Homsy, "Resonant Side-Band Instabilities in Wave Propagation in Fluidized Beds," *J. Fluid Mech.*, **122**, 433 (1982).
Ding, J., and D. Gidaspow, "A Bubbling Fluidization Model Using Kinetic Theory of Granular Flow," *AIChE J.*, **36**, 523 (1990).
Doedel, E., H. Keller, and J. Kernevez, "Numerical Analysis and Control of Bifurcation Problems. I: Bifurcation in Finite Dimensions," *Intl. J. Bifurcation Chaos*, **1**, 493 (1991).
Fan, L. S., and C. Zhu, *Principles of Gas-Solid Flows*, Cambridge University Press, New York (1998).
Fanucci, J. B., N. Ness, and R.-H. Yen, "On the Formation of Bubbles in Gas-Particulate Fluidized Beds," *J. Fluid Mech.*, **94**, 353 (1979).
Garg, S. K., and J. W. Pritchett, "Dynamics of Gas Fluidized Beds," *J. Appl. Phys.*, **46**, 4493 (1975).
Geldart, D., ed., *Gas Fluidization Technology*, Wiley, New York (1986).
Glasser, B. J., I. G. Kevrekidis, and S. Sundaresan, "One and Two-Dimensional Traveling Wave Solutions in Gas-Fluidized Beds," *J. Fluid Mech.*, **306**, 183 (1996).
Glasser, B. J., S. Sundaresan, and I. G. Kevrekidis, "From Bubbles to Clusters in Fluidized Beds," *Phys. Rev. Lett.*, **81**, 1849 (1998).
Goldhirsch, I., and G. Zanetti, "Clustering Instability in Dissipative Gases," *Phys. Rev. Lett.*, **70**, 1619 (1993).
Göz, M. F., "On the Origin of Wave Patterns in Fluidized Beds," *J. Fluid. Mech.*, **240**, 379 (1992).
Göz, M. F., "Transverse Instability of Plane Wavetrains in Gas-Fluidized Beds," *J. Fluid. Mech.*, **303**, 55 (1995).
Göz, M. F., and S. Sundaresan, "The Growth, Saturation, and Scaling Behavior of One and Two Dimensional Disturbances in Fluidized Beds," *J. Fluid. Mech.*, **362**, 83 (1998).
Harrison, S. E., and D. G. Crighton, "Solitons, Solitary Waves, and Voidage Disturbances in Gas-Fluidized Beds," *J. Fluid Mech.*, **266**, 233 (1994).
Hernandez, J. A., and J. Jimenez, *Bubble Formation in Dense Fluidized Beds*, *Proc. NATO Advanced Res. Workshop on the Global Geometry of Turbulence*, J. Jimenez, ed., Plenum Press, New York, 133 (1991).
Homsy, G. M., "Nonlinear Waves and the Origin of Bubbles in Fluidized Beds," *Appl. Scientific Res.*, **58**, 251 (1998).
Hrenya, C. M., and J. L. Sinclair, "Effects of Particle-Phase Turbulence in Gas-Solid Flows," *AIChE J.*, **43**, 853 (1997).
Jackson, R., "The Mechanics of Fluidized Beds. I: The Stability of the State of Uniform Fluidization," *Trans. Inst. Chem. Engrs.*, **41**, 13 (1963).
Jackson, R., "Progress Toward a Mechanics of Dense Suspensions of Solid Particles," *AIChE Symp. Ser.*, **90**, 1 (1994).
Jackson, R., "Locally Averaged Equations of Motion for a Mixture of Identical Spherical Particles and a Newtonian Fluid," *Chem. Eng. Sci.*, **52**, 2457 (1996).
Jackson, R., *The Dynamics of Fluidized Particles*, Cambridge University Press, New York (2000).
Johnson, P. C., and R. Jackson, "Frictional-Collisional Constitutive Relations for Granular Materials, with Application to Plane Shearing," *J. Fluid. Mech.*, **176**, 67 (1987).
Koch, D. L., and A. S. Sangani, "Particle Pressure and Marginal Stability Limits for a Homogeneous Monodisperse Gas-Fluidized Bed: Kinetic Theory and Numerical Simulations," *J. Fluid Mech.*, **400**, 229 (1999).
Kunii, D., and O. Levenspiel, *Fluidization Engineering*, Butterworth-Heineman, Oxford, U.K. (1991).
Liu, J. T. C., "Nonlinear Unstable Wave Disturbances in Fluidized Beds," *Proc. R. Soc. Lond. A*, **389**, 331 (1983).
Needham, D. J., and J. H. Merkin, "The Propagation of a Voidage Disturbance in a Uniformly Fluidized Bed," *J. Fluid Mech.*, **131**, 427 (1983).
Needham, D. J., and J. H. Merkin, "A Note on the Stability and the Bifurcation to Periodic Solutions for Wave-Hierarchy Problems with Dissipation," *Acta Mechanica*, **54**, 75 (1984a).
Needham, D. J., and J. H. Merkin, "On Roll Waves Down an Open Inclined Channel," *Proc. R. Soc. Lond. A*, **394**, 259 (1984b).
Needham, D. J., and J. H. Merkin, "The Existence and Stability of Quasi-Steady Periodic Voidage Waves in a Fluidized Bed," *Math. Phys. Z. Angew.*, **37**, 322 (1986).
Pai, S., and S. Luo, *Theoretical and Computational Dynamics of a Compressible Flow*, Van Nostrand Reinhold, New York (1991).
Pigford, R. L., and T. Baron, "Hydrodynamic Stability of a Fluidized Bed," *Ind. Eng. Chem. Fundam.*, **4**, 81 (1965).
Richardson, J. F., and W. N. Zaki, "Sedimentation and Fluidisation: 1," *Trans. Instn. Chem. Engrs.*, **32**, 35 (1954).
Sela, N., and I. Goldhirsch, "Hydrodynamic Equations for Rapid Flows of Smooth Inelastic Spheres, to Burnett Order," *J. Fluid Mech.*, **361**, 41 (1998).
Sokolichin, A., and G. Eigenberger, "Applicability of the Standard $\kappa - \epsilon$ Turbulence Model to the Dynamic Simulation of Bubble Columns: Part I. Detailed Numerical Simulations," *Chem. Eng. Sci.*, **54**, 2273 (1999).
Tsinontides, S., and R. Jackson, "The Mechanics of Gas Fluidized Beds with an Interval of Stable Fluidization," *J. Fluid Mech.*, **255**, 237 (1993).
Verloop, J., and P. M. Heertjes, "Shock Waves as a Criterion for the Transition from Homogeneous to Heterogeneous Fluidization," *Chem. Eng. Sci.*, **25**, 825 (1970).
Wallis, G. B., *One-Dimensional Two-Phase Flow*, McGraw-Hill, New York (1969).
Whitham, G. B., *Linear and Nonlinear Waves*, Wiley-Interscience, New York (1974).

Manuscript received Aug. 8, 2001, and revision received Feb. 25, 2002.